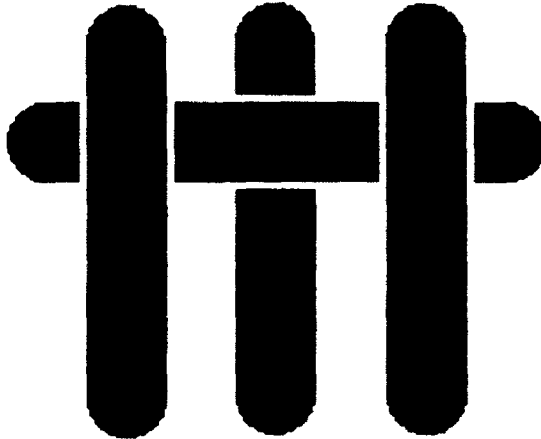


AD-A261 539

2



MATERIALS UCSB



ANNUAL REPORT to ONR

Contract Number: N00014-91-J-1875

DTIC  
ELECTE  
MAR 02 1993  
S E D

*Experimental Studies of Stress Measurement  
by Optical Fluorescence*

Principal Investigator:

David R. Clarke  
Materials Department  
University of California,  
Santa Barbara, CA 93106

93-04300



9048

December 1992

**RESTRICTION STATEMENT**  
Approved for public release  
Distribution Unlimited

3 01 82

## Summary Narrative.

In this program the measurement of stresses in ceramics using their optical fluorescence is being developed. The technique is based on the phenomena of piezo-spectroscopy, namely the shift in optical fluorescence of a material produced by a stress. In the course of the program to date we have a) derived for the first time a general relationship between an observed shift in fluorescence frequency and the state of stress, b) applied it to the determination of both applied and residual stresses in single crystal and polycrystalline materials, and c) begun to exploit the technique to the measurement of stresses in a variety of composite materials. These are described in detail in the accompanying technical reports appended here.

As part of this investigation we have also found that in ruby ( $\text{Cr}^{3+}$  doped sapphire) the observed optical fluorescence shift as a function of chromium concentration is a direct measure of the "image stress". This component of stress, originating from regions of mis-fit with the matrix, was introduced by Eshelby in the early 1950's but has not hitherto been measured directly. Although no application is yet evident to us, the measurement of the "image stress" does have an important place in the conceptual framework of the elasticity of inclusion and composite theory.

On-going work that has not yet reached completion includes:

a) development of a process for incorporating two different dopant species, each of which fluoresces at a different frequency. This is desirable since simultaneous fluorescence at different frequencies would facilitate the determination of the complete stress tensor. We have successfully demonstrated simultaneous fluorescence from two co-dopants but need now to measure the piezo-spectroscopic coefficients for the different dopants.

b) determination of the residual stresses in two-phase composites as a function of the volume fraction. Using the methodology developed in the first year, and described in report #1 attached, we have made measurements of the average residual stresses and the second moment of the stress distribution for a range of  $\text{Al}_2\text{O}_3\text{-ZrO}_2$  composites. We are now using an "information theory" approach to

relate these measurements to the thermal expansion coefficients and derive the temperature at which the thermal expansion stresses began to develop on cooling.

c) measurement of the stress distribution along embedded fibers in a composite from the shape of the fluorescence peak generated by a light beam propagating along and through an embedded fiber in a composite.

### List of Publications Describing Research Supported by Award N00014-91-J-1875

1. *Stress Measurement In Single and Polycrystalline Ceramics Using Their Optical Fluorescence*, Qing Ma and David R. Clarke, Journal of the American Ceramic Society, In Press.

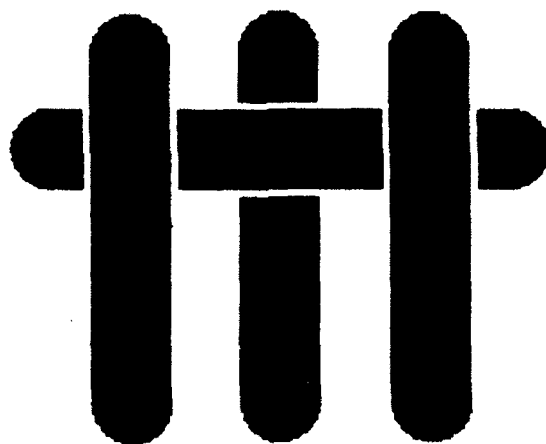
2. *Measurement of Residual Stresses in Sapphire Fiber Composites Using Optical Fluorescence*, Qing Ma and David R. Clarke, Acta Metallurgica et Materialia, In Press.

3. *Optical Fluorescence from Chromium Ions in Sapphire: A Probe of the Image Stress*, Qing Ma and David R. Clarke, Acta Metallurgica et Materialia, In Press.

4. *Residual Stresses In Al<sub>2</sub>O<sub>3</sub>-ZrO<sub>2</sub> Composites*, Qing Ma, Wolfgang Pompe and David R. Clarke, in preparation.

By _____	
Distribution/ _____	
Availability Codes	
Dist	Avail and/or Special
A-1	

**MATERIALS UCSB**



**Stress Measurement In Single and Polycrystalline  
Ceramics Using Their Optical Fluorescence**

by

**Qing Ma and David R. Clarke  
Materials Department  
University of California, Santa Barbara**

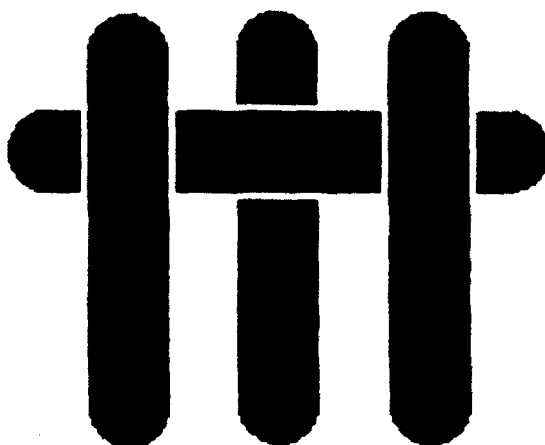
**A Technical Report for**

**Office of Naval Research**

**Contract No. N00014-91-J-1875**

**Principal Investigator: David R. Clarke  
Materials Department  
University of California**

# MATERIALS



## *STRESS MEASUREMENT IN SINGLE AND POLYCRYSTALLINE CERAMICS USING THEIR OPTICAL FLUORESCENCE*

Qing Ma and David R. Clarke

Materials Department  
University of California  
Santa Barbara, California 93106

### **Abstract**

A general methodology is developed for determining the state of stress and the numerical value of the stresses from observed shifts and broadening of optical fluorescence lines. The method is based on the piezo-spectroscopic properties of single crystals. We present general relationships between the measured fluorescence shifts and the stress state for a number of illustrative cases, pertinent to both polycrystalline and single crystal ceramics under stress. These include measuring the stresses applied to polycrystalline ceramics, the residual stress distribution due to crystallographically anisotropic thermal expansion, and the stresses applied to single crystals. Using the recently implemented technique of performing the fluorescence measurements in an optical microprobe, we also provide experimental tests of the relationships derived.

# 1 INTRODUCTION

Despite the importance of measuring the stress state in a material or structure there are few quantitative methods available. Those that have been developed and widely used, such as photoelastic methods and X-ray methods, whilst accurate are generally limited to examining flat surfaces and ones where the area interrogated is not obscured or shadowed by features such as steps. In addition they are difficult to apply to the measurement of stresses from small areas, a few microns across, and are not generally microscope-based thus precluding making measurements from features identifiable during examination of a microstructure.

For these, and related, reasons a number of optical techniques based on piezo-spectroscopic phenomena have been proposed. One gaining increased support, especially in VLSI silicon based technologies, is that of Raman spectroscopy using an optical microprobe [1]. The Raman lines of silicon at  $520\text{ cm}^{-1}$  are shifted by the application of a stress, and so regions on a silicon wafer around fine metal lines and dielectric features can be probed, with approximately a micron resolution, and their stress evaluated. Another piezo-spectroscopic technique proposed in the late 1970's for the measurement of stress, is that of fluorescence spectroscopy [2]. The suggestion, made by Grabner, followed the demonstration at the Bureau of Standards that the pressure in high-pressure experimental cells could be calibrated by the shift of the chromium fluorescence lines from fine particles of ruby embedded in the high-pressure cell [3]. In turn, this work built on the luminescence studies of chromium doped sapphire by Schawlow [4] and, independently by Sugano and Tanabe [5], as part of their investigation of possible laser materials. They found that the luminescence lines in chromium-doped sapphire were shifted by an applied stress. We have recently demonstrated that by implementing the fluorescence spectroscopy using an optical microprobe it is pos-

sible to measure stresses in chromium-doped alumina from regions identified in the optical microscope and with a spatial resolution of a few microns [6].

In this paper we present a method of analyzing an observed frequency shift in terms of the piezo-spectroscopic coefficients and the stress (and hence strain) on the crystal structure containing a fluorescing atom. This provides a correction to the equation derived by Grabner for the case of chromium fluorescence in alumina [2]. We then extend the analysis to the measurement of stresses in inhomogeneously stressed materials, presenting a number of illustrative examples of the application of the fluorescence technique to the measurement of commonly occurring types of stresses in ceramics. These provide the basis for future work in the widespread application of the technique to measure stresses in ceramic composites and at ceramic interfaces.

## **2 PRINCIPLES OF PIEZO-SPECTROSCOPIC ANALYSIS**

The basis of all piezo-spectroscopic methods for the measurement of stress in crystalline materials is that an applied stress strains the lattice and alters the energy of transitions between electronic or vibrational states. In this way, the energy of any radiative transitions, such as those that give rise to luminescence, also varies and produces systematic shifts in the frequency of luminescence lines such as fluorescence lines. In common with other spectroscopies, the sharpness of the fluorescence line depends on temperature and variations in the site position of the fluorescing atomic species. When the fluorescing ion is located on a lattice site in a tightly bound, high elastic modulus material, as is the case for chromium substitution for an aluminum ion in the sapphire lattice, the lines can be exceptionally sharp, broadened only by phonon scattering. Interstitial dopants, where there is greater variability in the dopant site or in a random network structure, such as chromium in glasses, give rise

to much broader, and usually weaker, luminescence lines.

The principle of relating an observed line shift in a fluorescence or absorption spectrum to the state of stress have been described previously by Grabner [2] in reference to the measurement of stresses in sintered, polycrystalline alumina containing a trace of  $\text{Cr}^{3+}$ . The more general case is presented here.

When a crystal is subject to a homogeneous stress  $\sigma_{ij}^*$  (in crystallographic frame of reference), the change in frequency,  $\Delta\nu$ , of a luminescence line is given by the tensorial relationship:

$$\Delta\nu = \Pi_{ij} \sigma_{ij}^* \quad (1)$$

where  $\Pi_{ij}$ 's are the piezo-spectroscopic coefficients relating frequency to stress. They form symmetrical second rank tensors, which have symmetry properties governed by the point symmetry group of the fluorescing ion. They may also have different numerical values for different fluorescence line energies. No appreciable stress induced broadening has been reported at room temperature so the lines merely shift with stress without changing shape. (Stress induced splitting is detectable at liquid helium temperatures but is unobservable at room temperature being masked by thermal broadening). In general, any applied stress will not be imposed on the crystal along its crystallographic axes, as represented in equation 1, but rather in some other coordinate frame. The stress on the crystal structure will then be given by the applied stress components resolved onto the crystallographic axes, i.e. through an orthogonal coordinate transformation:

$$\sigma_{ij}^* = a_{ik} a_{jl} \sigma_{kl} \quad (2)$$

where  $a_{ij}$  is the transformation matrix relating the frame of reference in which the applied

stresses are defined with respect to the crystallographic axes of the lattice.

Thus, the frequency shift of a fluorescence line in a luminescing crystal oriented at an arbitrary angle to a superimposed stress and strain field is given by the following tensorial relation:

$$\Delta\nu = \Pi_{ij} a_{ik} a_{jl} \sigma_{kl} = \Pi_{ij} c_{ijkl} a_{km} a_{ln} \epsilon_{mn} \quad (3)$$

One of the major limitations of piezo-spectroscopy is evident from this equation. Unless the fluorescing species emits at several different frequencies, so that a set of simultaneous equations (one for each transition) can be generated, there may be an insufficient number of distinct transitions to solve for each of the maximum of six independent stress components needed to completely describe the stress state. In some materials, the point symmetry of the fluorescing ion may also preclude the determination of all the independent stress components. This will be seen to be the case for both MgO and Al<sub>2</sub>O<sub>3</sub>.

Of the many fluorescence spectra reported, that of chromium fluorescence in sapphire has probably been the most thoroughly studied. The chromium ions replace aluminum ions substitutionally in the sapphire lattice and maintain their trivalent state, Cr<sup>3+</sup>. Although the chromium ion is surrounded by an octahedron of oxygen ions, the octahedron is distorted along the body diagonal giving a point symmetry of D<sub>3d</sub>( $\bar{3}m$ ) for the chromium ion. The distortion also causes an asymmetry of the electrostatic crystal-field and results in a splitting of the <sup>2</sup>E energy levels by 0.004 eV, in turn giving rise to the two distinct radiative transition lines in ruby, R<sub>1</sub> and R<sub>2</sub> at 1.790 and 1.794 eV respectively. From the point symmetry of the chromium ion, it can be shown that the off-diagonal components of the piezo-spectroscopic tensor are zero and that the diagonal components are symmetrical about the c-axis, namely  $\Pi_{11} = \Pi_{22} \neq \Pi_{33}$ . For simplicity, we will use  $\Pi_{11} = \Pi_{22} = \Pi_a$  and  $\Pi_{33} = \Pi_c$  for R<sub>1</sub> and R<sub>2</sub>

lines. Substituting these components into equation 3, the frequency shift for a chromium fluorescence line can be expressed in terms of the applied stress components as:

$$\begin{aligned} \Delta\nu = & \Pi_a(\sigma_{11} + \sigma_{22} + \sigma_{33}) + (\Pi_c - \Pi_a)(a_{31}^2 \sigma_{11} + a_{32}^2 \sigma_{22} + a_{33}^2 \sigma_{33}) \\ & + 2(\Pi_c - \Pi_a)(a_{31}a_{32} \sigma_{12} + a_{32}a_{33} \sigma_{23} + a_{31}a_{33} \sigma_{31}) \end{aligned} \quad (4)$$

This differs from the expression derived by Grabner (equation 4 reference 2) in having an additional term (the second) proportional to the trace of the applied stress tensor. For the particular case in which the applied stress is purely hydrostatic, this equation simplifies to that used in the high-pressure physics and materials literature, namely

$$\Delta\nu = -(2\Pi_a + \Pi_c)P \quad (5)$$

where  $P$  is the pressure. Also, unlike Grabner's equation, equation 4 reduces to equation 1 when the stress field is applied along the crystal axes. The point symmetry of the chromium ion simplifies equation 3 but nevertheless the stress components cannot be determined completely from the shifts of the  $R_1$  and  $R_2$  lines unless the misorientation between the applied stress and the crystal axes is known from some other, independent measurement.

The chromium fluorescence spectrum from magnesia has also been investigated in some detail [7], and can similarly be used to monitor strains. As in sapphire, the chromium ion occupies substitutionally a lattice site in magnesia and is surrounded by an octahedron of oxygen ions. However, the oxygen octahedra remain undistorted so the chromium point symmetry is raised to  $m\bar{3}m$ . As a consequence, the  ${}^2E$  level is not split and only one line, at  $14319 \text{ cm}^{-1}$ , occurs. The  $m\bar{3}m$  point symmetry imposes the additional requirement that the diagonal piezo-spectroscopic coefficients are all equal ( $\Pi_{11} = \Pi_{22} = \Pi_{33}$ ). Thus, for

chromium luminescence in magnesium oxide, the line shift is sensitive only to the trace of the stress tensor:

$$\Delta\nu = \Pi_{11}(\sigma_{11} + \sigma_{22} + \sigma_{33}) \quad (6)$$

This insensitivity to the deviatoric stresses, nevertheless, has the advantage that the shift is independent of the orientation of the crystal structure with respect to the applied stress.

Rare earth ions, such as  $\text{Sm}^{3+}$  and  $\text{Nd}^{3+}$ , can substitute for the yttrium ion in the yttrium aluminum oxide, garnet structure and give rise to sharp characteristic fluorescence spectra. The six possible substitutional sites, although equivalent under the cubic point group symmetry of YAG, have orthorhombic site symmetry. Since ions at all three sites will fluoresce when the crystal is excited, applying a stress should in general break the degeneracy associated with the equivalence of the three sites and cause line splitting. However, in practice, the stress splitting is masked by thermal broadening at room temperature, and so the fluorescence appears to come from a crystal having cubic symmetry [8] with equal piezo-spectroscopic coefficients.

### 3 INHOMOGENEOUS STRAIN FIELDS

The above analysis pertains to the case of a single crystal subject to a homogeneous strain field over the volume of material exposed to the excitation probe. When the probed volume contains more than one crystallite or the strains vary within it, the observed spectral shifts are more complex. They can, however, be understood from simple superposition arguments provided inelastic scattering of the luminescence is not appreciable and the strains do not vary over distances comparable to the lattice spacing. (For the case of the N- and F- fluorescence lines, the latter requirement is a little more stringent. In that case, the strains should not

vary over distances associated with the separation of the ions making up the chromium pairs from which these characteristic lines originate).

Subject to these restrictions, strain inhomogeneities and the presence of multiple grains within the probed volume can cause both broadening and shifting of the luminescence lines as analyzed in Appendix A. In essence, each element of material over which there is a constant crystallographic orientation and homogeneous strain contributes a signal intensity proportional to its volume and concentration of fluorescence ions. The spectral shift is given by equation 3 with the appropriate values for each of the parameters. The superposition of the lines, shifted according to the strain of each volume element, causes the observed line to appear to be broadened and shifted. The broadening is not a measure of the deviatoric strains per-se as has been stated in the literature previously [2] but rather of the statistical variation in strains and crystallographic orientations in the region examined. As a result the broadening need not be symmetrical. Indeed the broadened lines can have a fine structure resulting from there being one or two regions whose contributions are disproportionately large. This is probably the cause of the fine structure in the spectra reported by Grabner [2].

Although analytical relationships between line shifts, broadening and inhomogeneous stress state in polycrystalline materials can not, in general, be presented, a number of simple cases of practical importance can be considered. Equations for a number of these are derived as described in the following sub-sections.

### **3.1 Polycrystalline Material**

The first example for which an analytical function can be derived corresponds to a polycrystalline material, with no crystallographic texture or internal residual stress, under a

homogeneous applied stress and probed with an excitation beam large compared to the grain size. In this case, the contributions from the individual crystallites are averaged over many, randomly oriented grains.

The frequency shift in the fluorescence line is given by the first moment of the distribution of fluorescence frequencies. Using equations 3, and A6 and B3 in the appendices, this can be simply expressed as:

$$\overline{\Delta\nu} = \iiint P(\theta, \phi, \psi) \Delta\nu d\theta d\phi d\psi$$

which reduces to

$$\overline{\Delta\nu} = \frac{1}{3} (\Pi_{11} + \Pi_{22} + \Pi_{33})(\sigma_{11} + \sigma_{22} + \sigma_{33}) \quad (7)$$

This equation shows that, irrespective of the crystal structure, the frequency shift of the fluorescence from a large number of grains in a polycrystalline material is dependent only on the trace of the applied stress tensor.

The polycrystalline ensemble of grains also leads to an intrinsic, stress dependent broadening of the fluorescence line. The peak broadening is given by the second moment of the distribution, which using equation A8, may be written as:

$$\begin{aligned} \langle \Delta\nu^2 \rangle &= \frac{4}{15} \left[ (\Pi_{22} - \Pi_{11})^2 + (\Pi_{33} - \Pi_{11})^2 - ((\Pi_{22} - \Pi_{11})(\Pi_{33} - \Pi_{11})) \right] \\ &\times \left[ \frac{1}{3} (\sigma_{11}^2 + \sigma_{22}^2 + \sigma_{33}^2 - \sigma_{11}\sigma_{22} - \sigma_{22}\sigma_{33} - \sigma_{33}\sigma_{11}) + (\sigma_{12}^2 + \sigma_{23}^2 + \sigma_{31}^2) \right] \quad (8) \end{aligned}$$

Such broadening is due to the differences in the diagonal piezo-spectroscopic coefficients. Consequently, for materials with fluorescing ions having cubic point symmetry, such as  $\text{Cr}^{3+}$  in MgO, (for which the piezo-spectroscopic coefficients are equal) the application of an external stress does not cause any broadening.

### 3.2 Inhomogeneously Stressed Single Crystal

The second case corresponds to a single crystal containing inhomogeneously stressed regions. A special case, but nevertheless an important one, is one in which the stress varies with depth below the surface, such as might pertain to surface stressing produced by ion exchange or when the sample is loaded in bending. For purposes of generality, we may assume that the concentration of the fluorescing ion,  $c$ , is a function of depth  $z$ . We can, in principle, also incorporate various instrumental functions, such as the collection efficiency as a function of depth of the apparatus used to measure the fluorescence spectrum, into a function  $g(z)$ . The function  $g(z)$  allows the fluorescence signal to be normalized:

$$\int c(z)g(z)dz = 1$$

and a weighting function introduced:

$$W(\Delta\nu)d\nu = c(z)g(z)dz \quad (9)$$

Again, for purposes of generality, the frequency shift can be written so as to include a shift dependent on the concentration,  $c$ , of the fluorescing species:

$$\Delta\nu = \Pi_{i,j} a_{ik}a_{jl} \sigma_{kl} + \beta(c - c_0) \quad (10)$$

where  $c_0$  is the concentration of the reference sample which the shift is compared.

The average peak shift, expressed by the first moment of the fluorescence peak then becomes

$$\overline{\Delta\nu} = \int [\Pi_{i,j} a_{ik}a_{jl} \sigma_{kl} + \beta(c - c_0)] c(z)g(z)dz \quad (11)$$

The broadening is a mixture of the inhomogeneous broadening due to the depth dependence of shift and the intrinsic homogeneous broadening due to change of concentration. For simplicity, we give the result for the case of constant concentration  $c_0$ :

$$\langle \Delta\nu^2 \rangle = \int (\prod_{ij} a_{i,k} a_{j,l} \sigma_{kl})^2 c_0 g(z) dz - \overline{\Delta\nu}^2 \quad (12)$$

in which  $\overline{\Delta\nu}^2$  is also evaluated at  $c = c_0$ .

### 3.3 Anisotropic Thermal Expansion Residual Stresses

The third case considered here is of a polycrystalline material for which the thermal expansion coefficient is crystallographically anisotropic. As a result of such thermal expansion anisotropy, residual stresses can be created on cooling from the fabrication temperature, with the magnitude of the stresses being dependent on the geometrical constraint imposed by the neighboring grains, the elastic properties of the grains and the extent to which accommodation mechanisms, such as creep and plastic deformation, which can relax the stresses. In the special cases in which the grains do not constrain one another on cooling or the accommodation mechanisms are complete, no internal stresses develop and neither a line shift nor broadening would arise. However, there is in general some mutual constraint imposed by the contracting grains that causes stresses to develop within the material. The average stress over the material must be zero but variations in stress from one grain to another can cause both a broadening of the line and a line shift. Although the specific values will vary from place to place in the sample, since the stresses will also vary from grain to grain, it is possible to calculate the average values as will now be shown. Two assumptions are made. First, that the probed volume encompasses a sufficiently large number of grains that an ensemble average can be considered, and secondly that the distribution of stresses can be described

by an appropriate distribution function.

Consider a material, such as alumina, which has a thermal expansion coefficient that is larger along its  $c$ -axis than along its  $a$ -axis, and has an axis of rotational symmetry along the  $c$ -axis. On cooling from its fabrication temperature, tensile stresses will, on average, develop along the  $c$ -axis of the grains and compressional stresses will develop in the basal plane. Therefore,

$$\bar{\sigma}_a < 0, \quad \bar{\sigma}_c > 0 \quad (13)$$

Now, consider a grain intersected by an arbitrarily placed plane that divides the polycrystalline sample into two. The orientation of the grain can be specified by the angular coordinates  $(\theta, \phi)$  of its  $c$ -axis (figure 1). Provided the dividing plane intersects a large number of grains, with all possible stress states, we need only consider the average stresses along the  $a$ - and  $c$ - axes. Therefore the stress in the basal plane is equi-biaxial, and rotation of the grain around the  $c$ -axis does not alter its stress state. The force acting per unit area in any grain perpendicular to the dividing plane can be expressed by resolving the stresses in that grain:

$$f = \bar{\sigma}_a \sin^2 \theta + \bar{\sigma}_c \cos^2 \theta \quad (14)$$

Since, across the dividing plane, the orientation of the grains is random, the average force can be written as:

$$\bar{f} = \frac{1}{2\pi} \int_0^{2\pi} d\phi \int_0^{\pi/2} f \sin \theta d\theta \quad (15)$$

Since the force must on average be zero,  $\bar{f} = 0$ , the mean stresses in the  $c$ - and  $a$ - crystallographic directions are related by:

$$\bar{\sigma}_c = -2\bar{\sigma}_a \quad (16)$$

Recognize that the average stresses described above are equivalent to volume average, the mean shift of the fluorescence line is therefore,

$$\overline{\Delta\nu} = (\Pi_c - \Pi_a)\overline{\sigma_c} \quad (17)$$

The peak broadening can be calculated using equation A8 on the assumption that the distribution in stresses in the *a*- and *c*- crystallographic directions are independent of one another:

$$P(\sigma_a, \sigma_c) = p(\sigma_a)p(\sigma_c) \quad (18)$$

and are also Gaussian with the same width,  $\sigma_w$

$$p(\sigma_a) = \frac{1}{\sqrt{2\pi}\sigma_w} \exp\left[-\frac{(\sigma_a - \overline{\sigma_a})^2}{2\sigma_w^2}\right] \quad (19)$$

The assumption of independence of the stress distributions in the different directions enables the weighting function in equation A8 to be written as:

$$W(\Delta\nu)d\nu = P(\sigma_a, \sigma_c)d\sigma_a d\sigma_c = p(\sigma_a)p(\sigma_c)d\sigma_a d\sigma_c$$

So, the peak broadening becomes:

$$\langle \Delta\nu^2 \rangle = 4\Pi_a^2 \sigma_w^2 + \Pi_c^2 \sigma_w^2 \quad (20)$$

Thus, using measurements of the mean peak shift, which from equation 17 gives the mean stresses along the *a*- and *c*- axes, and a measurement of the peak width, the stress distribution within the material can be determined.

These equations shows that the crystallographic anisotropy in thermal expansion leads to both an average shift and broadening of the fluorescence line. They are related to the average values of the stresses and the stress distribution. The spatially varying stresses can be significantly larger than the average, especially those acting over smaller distances than the grain size, related to the presence of the grain edges and corners. These are primarily responsible, for instance, for micro-crack extension. Although detailed information of such stresses does not appear to be amenable to the analysis of the shape of the fluorescence lines, their magnitude and the occurring frequency are reflected by the stress distribution.

### 3.4 Matrix Stresses Due to Presence of Fibrous Inclusions

The final case considered is that of a polycrystalline matrix surrounding an embedded fiber. The radial and tangential stresses in a matrix around a misfitting fiber of radius,  $r_0$ , are given by standard elastic solutions, varying with the inverse square of distance,  $r$ , from the fiber axis. For observations made in a cross-section perpendicular to the fiber axis (axis 3), the matrix stresses may be written as

$$\sigma_{11} = -\sigma_{22} = \frac{\sigma_0 r_0^2}{r^2}; \quad \sigma_{33} = 0 \quad (21)$$

Thus, from equation 3, the frequency shifts are given by

$$\Delta\nu = (\Pi_{22} - \Pi_{11})(a_{21}^2 - a_{22}^2)\sigma_{11} + (\Pi_{33} - \Pi_{11})(a_{31}^2 - a_{32}^2)\sigma_{22} \quad (22)$$

which would be detectable with a probe having high optical resolution ( $\ll r_0$ ). If the probe is large, such that either many grains in a polycrystalline matrix or regions within a circle encompassing the fiber in a single crystal matrix are excited simultaneously, then the average

peak shift is  $\overline{\Delta\nu} = 0$ . The peak broadening, for such a large probe, would also average out for single crystal and polycrystalline material to a value of

$$\langle \Delta\nu^2 \rangle = \frac{4}{45} \overline{\sigma_{11}^2} [(\Pi_{22} - \Pi_{11})^2 + (\Pi_{33} - \Pi_{11})^2 - (\Pi_{22} - \Pi_{11})(\Pi_{33} - \Pi_{11})] \quad (23)$$

where  $\overline{\sigma_{11}^2}$  is averaged over the volume probed.

## 4 OBSERVATIONAL TESTS

In this section a series of measurements are described that provide experimental tests and validations of the equations presented in the preceding sections. The tests were made with aluminum oxide because of its ready availability. The experiments were performed using an unmodified optical microprobe<sup>1</sup> to both excite the luminescence and to collect and analyze the resulting fluorescence spectrum using an attached spectrometer. (The optics of the Microprobe have been described in an earlier publication [9]). A number of laser frequencies have been used to excite the luminescence but the results reported here were all obtained using an argon ion laser with a wavelength of 514 nm. The experimental procedure was to select a region of interest on the sample with the attached optical microscope, focus the laser beam to a spot on the selected feature and analyze the fluorescence produced. The intensity of the  $R_1$  and  $R_2$  fluorescence lines were typically scanned by integrating over 0.5 second intervals at a spacing of 0.2 wavenumbers, with the intensities being recorded under computer control. The collected data were subsequently analyzed with curve fitting algorithms, included in the LabCalc software package<sup>2</sup>, to identify the position of the fluorescence peak. By using objective lenses of 50 $\times$  and 100 $\times$  magnifying powers minimum spot sizes of  $\sim 5\mu\text{m}$

<sup>1</sup> Instruments SA, Raman Microprobe Model T64000.

<sup>2</sup> Galactic Industries Corp.

and  $\sim 1 - 2\mu\text{m}$  can be produced. Larger probe sizes were formed by partial defocusing. Also, by appropriate choice of the collection aperture size, the attainable axial resolution could be varied by the collection optics from  $\sim 10\mu\text{m}$  to  $\sim 200\mu\text{m}$  [10].

All the measurements were made with the sample at room temperature. Although a change in temperature is known to cause a line shift of  $\sim 0.14\text{ cm}^{-1}/^{\circ}\text{C}$  [11] (to smaller wavenumbers with increasing temperature), no line shift was noted when the spot size was systematically decreased (thereby increasing the power density incident on the sample) indicating that no significant heating of the probed volume occurred. This lack of sensitivity to spot size was attributed to both the low absorption of ruby at the excitation frequencies and the relatively low illumination intensities used. Variations were, however, noted with variations in room temperature and so corrections were made to the peak shifts. This involved corrections for the change in room temperature using the above temperature dependence of line frequency and changes of the spectrometer dimensions as a result of thermal expansion. The latter was corrected by simultaneously monitoring a characteristic Neon line at  $14431\text{ cm}^{-1}$ .

#### 4.1 Polycrystalline Sample Under Stress

In order to test the validity of equations 7 and 8 concerning the stress dependence of the peak shift and broadening in a polycrystalline material, polished bars of polycrystalline alumina (Coors AD96) were subject to an applied stress and the fluorescence spectra recorded. The stress was applied using a four-point bend stage specially designed to fit under the optical microscope of the microprobe. The polycrystalline alumina contained sufficient levels of chromium impurity to provide sufficiently strong fluorescence peaks to be analyzed. In order to average over many grains, a probe diameter of  $\sim 50\mu\text{m}$  was used for the fluorescence

measurements. The grain size of the alumina was 2-20 $\mu$ m.

Since alumina is thermally anisotropic, the analysis in section III.1 has to be extended to separate the effect of thermal residual stress existing in the sample from any applied stress. The shift from a small volume element  $dv$  (much smaller than the grain size) is

$$\Delta\nu = 2\Pi_a(\sigma_a^A + \sigma_a^T) + \Pi_c(\sigma_c^A + \sigma_c^T) \quad (24)$$

where the superscripts  $A$  and  $T$  denote applied and thermal stresses respectively. Since the above equation is linear, the effects of two types of stress can be separated:

$$\Delta\nu = \Delta\nu^A + \Delta\nu^T \quad (25)$$

Therefore, the mean shift:

$$\overline{\Delta\nu} = \frac{1}{V} \int (\Delta\nu^A + \Delta\nu^T) dv = \overline{\Delta\nu^A} + \overline{\Delta\nu^T} \quad (26)$$

Since the shift generated by thermal stress (see section 4.3) can be measured independently,  $\overline{\Delta\nu^A}$  can be obtained.

The broadening is calculated by using equation A8:

$$\begin{aligned} \langle \Delta\nu^2 \rangle &= \frac{1}{V} \int (\Delta\nu^A + \Delta\nu^T)^2 dv - \overline{\Delta\nu}^2 \\ &= \langle (\Delta\nu^A)^2 \rangle + \langle (\Delta\nu^T)^2 \rangle + 2 \left[ \overline{\Delta\nu^A \Delta\nu^T} - \overline{\Delta\nu^A} \overline{\Delta\nu^T} \right] \end{aligned} \quad (27)$$

So the broadening can be separated provided that  $\Delta\nu^A$  and  $\Delta\nu^T$  are uncorrelated.

The measured peak shifts for the  $R_1$  and  $R_2$  fluorescence lines as a function of applied stress are shown in figure 2. The lines through the data, fitted by a least square analysis,

shows that the stress dependence of the shift of the  $R_1$  and  $R_2$  fluorescence lines is 2.46 and 2.50  $\text{cm}^{-1}\text{GPa}^{-1}$  respectively. The fit coefficient  $R$  is 0.997 for both lines. For comparison to the theory in section III.1, equation 7 would predict that when a uniform stress is applied to polycrystalline alumina, the peak shift would be given by:

$$\overline{\Delta\nu} = \frac{1}{3} (2\Pi_a + \Pi_c) \sigma^A$$

Using the hydrostatic pressure dependence of peak shifts for the  $R_1$  and  $R_2$  lines given by Munro *et. al.* [12], the sum of the spectroscopic coefficients,  $2\Pi_a + \Pi_c$  have the values of 7.59 and 7.62  $\text{cm}^{-1} \text{GPa}^{-1}$  for the  $R_1$  and  $R_2$  lines respectively. The peak shifts of the  $R_1$  and  $R_2$  lines would then be 2.53 and 2.54  $\text{cm}^{-1}\text{GPa}^{-1}$ , close to that observed. The uniaxial compression experiment by Feher and Sturge [13] provided values for  $\Pi_a$  and  $\Pi_c$  independently with values of 2.7 and 2.15  $\text{cm}^{-1} \text{GPa}^{-1}$  for both  $R_1$  and  $R_2$  lines. Using these data, the predicted stress dependence would be 2.52  $\text{cm}^{-1}\text{GPa}^{-1}$ , again close to that observed. We can therefore conclude that our measured shifts fall within the uncertainty of the existing data on the piezo-spectroscopic coefficients.

The measured peak widths for the  $R_1$  and  $R_2$  fluorescence lines as functions of applied stress are shown in figure 3. For this material the systematic broadening due to the applied stress of both lines is small compared to the variability from one point on the sample to another.

#### 4.2 Single Crystal With Surface Stress

A single crystal treated to produce a surface stress represents a special case of the inhomogeneously stressed single crystal considered in section III.2. To provide an experimental test of the effect of inhomogeneous stressing, a residual surface stress was produced in a single

crystal of *c*-axis sapphire by in-diffusion of chromium and the fluorescence measured as a function of an applied stress. Since chromium oxide, Cr<sub>2</sub>O<sub>3</sub>, is isostructural with Al<sub>2</sub>O<sub>3</sub> but has a larger lattice parameter, diffusion of chromium into the surface of Al<sub>2</sub>O<sub>3</sub> is expected to produce a compressive surface stress.

As chromium is both the fluorescing ion and the ion causing the surface stress, the analysis of section III.2 must include the stress created by the in-diffusion of chromium. In this case, the frequency shift is expected to be the sum of three distinct contributions, that due to any applied stress, that due to diffusion-induced stresses  $\sigma^D$  and that due to variations in fluorescing ion concentrations:

$$\Delta\nu = \Pi_{ij} \sigma_{ij}^A + \Pi_{ij} \sigma_{ij}^D + \beta(c - c_0) \quad (28)$$

The overall peak shift from the in-diffused layer can be written as:

$$\overline{\Delta\nu} = \int \Delta\nu c(z)g(z)dz = \overline{\Delta\nu^A} + \overline{\Delta\nu^D} + \overline{\Delta\nu^C} \quad (29)$$

Since the frequency shift in equation 28 is the sum of the individual components, the mean peak shifts of each component are also linearly independent as shown by equation 29. Thus, in an experiment in which an external stress is applied to a residually stressed surface, the mean frequency shift observed is predicted to be due to the applied stress only:

$$\overline{\Delta\nu^A} = \int \Delta\nu^A c(z)g(z)dz = \Pi_{ij} \overline{\sigma_{ij}^A} \quad (30)$$

For four-point bending, the applied stress is essentially constant over the depth of the in-diffused layer, and so the mean frequency shift will be linearly related to the applied

stress.

For the experiment, in-diffusion of chromium was performed in a three step process. In the first step, a chromium acetate solution was spun-coated onto a *c*-axis oriented sapphire disc. The coating was then pyrolyzed and oxidized by heating to 600°C in air. Then, finally, the disc was annealed at 1600°C to diffuse in the chromium and beams cut from the disc. To investigate the effect of applied stress the sapphire beam was loaded in four-point bending with *c*-axis perpendicular to the loading plane, placed under the microscope of the microprobe, and the resulting fluorescence recorded as a function of load. The observed peak shift for the  $R_1$  and  $R_2$  lines as a function of applied stress is shown in figure 4. For these data, the stress dependence is 2.42 and 2.61  $\text{cm}^{-1}\text{GPa}^{-1}$  for the  $R_1$  and  $R_2$  lines respectively, which compares favorably to the mean  $\Pi_a$  value of 2.7  $\text{cm}^{-1}\text{GPa}^{-1}$  given in [13]. The fit coefficient  $R$  equals 0.996 and 0.994, respectively.

### 4.3 Thermal Expansion Anisotropy Stresses

Residual stresses are known to be produced in polycrystalline alumina on cooling as a result of the crystallographic anisotropy in thermal expansion coefficients along the *c*- and *a*- axes. In order to measure the average residual stresses, the fluorescence from three different sintered, polycrystalline aluminas (Coors AD96, Coors AD 995 and UCSB1) and a polycrystalline alumina hiped at UCSB (UCSB2) was recorded using an excitation probe diameter of 50 $\mu\text{m}$ . The UCSB1 material is a high purity alumina sintered at 1800°C for 1 hr. in hydrogen. The probe size was much larger than the grain size of the ceramics, assuring that the fluorescence was being averaged over a large number of grains. The ceramic samples contained an adequate chromium impurity level for the  $R_1$  and  $R_2$  fluorescence peaks to be recorded with sufficient signal-to-background ratio that precise measurements could be made

of the peak shape and peak shift. The peak shift and peak broadening were measured relative to those recorded from a polished single crystal of sapphire that also contained a trace level of chromium impurity. For comparison, the spectrum obtained from the AD995 sample is plotted together with that of a single crystal sapphire in Figure 5. Several spectra were taken at different spots for each sample, the average peak shifts and broadening for the samples are listed in table I. Also shown in the table are the average stresses,  $\bar{\sigma}_a$ ,  $\bar{\sigma}_c$  and the breadth of stress distribution  $\sigma_w$  calculated using equations 16, 17 and 20 above.

## 5 CLOSING REMARKS

The preceding analyses and experiments illustrate how the technique of fluorescence spectroscopy can be used to make measurements of commonly arising types of stresses in ceramics. This is possible, despite the fact that the fluorescence shift is a scalar quantity whereas the complete stress state is tensorial, because considerable simplification of the equations (equation 3) can be made in many practical situations. For instance, stresses can be applied at prescribed orientations to the crystallographic axes of single crystals. Also, the polycrystalline nature of many ceramics enables the effects of crystallographic orientation to be averaged out. For instance, as equation 7 demonstrates, the frequency shift from a stressed polycrystalline ceramic is independent of its crystal structure and is only dependent on the trace of the applied stress.

Two of the analytical results are of particular interest. One, is the finding that the fluorescence shift is dependent only on the applied stress and not on the residual stresses produced by either thermal expansion mismatch as in the case of polycrystalline  $Al_2O_3$ , or by ion in-diffusion as in the case of  $Cr^{3+}$  in-diffusion into sapphire single crystal. The later

also suggests that a fluorescent dopant ion can be deliberately introduced into a structure or material to monitor the applied stress through changes in the fluorescence frequency. In fact, we have been utilizing this characteristics to make measurements of stresses in metal-ceramic laminates [14].

The second notable result concerns the measurement of the residual stresses due to anisotropic thermal expansion. The analysis indicates that the mean stress in the *a*- and *c*- crystallographic directions in aluminum oxide can be obtained from the mean frequency shift, and that the distribution in internal stresses can also be determined. These results represent an advance on previous studies of anisotropic thermal expansion stresses in aluminum oxide [2,15]. As already mentioned, Grabner's work led to an incomplete expression for the relationship between the frequency shift and stress, and so the values he derived are probably unreliable. The work of Blendell and Coble [15], was primarily concerned with the diffusional relaxation of the anisotropic thermal expansion stresses. They assumed an average stress in the material and calculated its relaxation for different grain sizes and cooling rates. They did not relate this average stress to any of the crystallographic stresses nor did they describe how they determined this average stress from their fluorescence observations. However, the measurements in table I indicate that the mean stresses in the samples of polycrystalline alumina examined are similar in magnitude to those calculated.

## ACKNOWLEDGEMENT

This work was supported by the U. S. Office of Naval Research under contract number N00014-91-J-1875.

## APPENDIX

### A Peak Shifts and Broadening due to Stresses

If the probed volume were strain free, the fluorescence peaks would be Lorentzian in shape and have a breadth dependent only on the finite temperature of the sample. The presence of stresses, however, causes the peaks to be shifted and dispersed as shown in the following.

Let the peak shape in the unstrained crystal be represented by the frequency function,  $f(\nu)$ , with the peak centroid given by:

$$\nu_c = \int f(\nu)\nu d\nu \quad (\text{A1})$$

and the area of the peak is normalized to be unity:

$$\int f(\nu)d\nu = 1 \quad (\text{A2})$$

The dispersion of the peak, corresponding to the peak width, can be expressed by the second moment of the distribution:

$$\langle \nu^2 \rangle_0 = \int f(\nu)(\nu - \nu_0)^2 d\nu \quad (\text{A3})$$

The effect of any stress distribution can be related to measured peak shape by assuming that the probability of causing a frequency shift,  $\Delta\nu$ , can be expressed as a weighting function  $W(\Delta\nu)$ . The resulting peak is then given by the function:

$$F(\nu) = \int f(\nu - \Delta\nu)W(\Delta\nu)d\Delta\nu \quad (\text{A4})$$

Since  $\int W(\Delta\nu)d\Delta\nu = \int F(\nu)d\nu = 1$  the area under the peak is conserved.

The centroid, or mean value, of the peak from the stressed volume is given by the first moment of the function representing the peak:

$$\nu_c = \int F(\nu)\nu d\nu \quad (\text{A5})$$

The peak shift is then:

$$\begin{aligned} \overline{\Delta\nu} &= \nu_c - \nu_0 \\ &= \int \Delta\nu W(\Delta\nu)d\Delta\nu \end{aligned} \quad (\text{A6})$$

As spectra  $f(\nu)$  and  $F(\nu)$  can be obtained from unstressed and stressed regions, the mean shift  $\overline{\Delta\nu}$  can be determined and from that the stress deconvoluted.

The width of the stress broadened peak,  $F(\nu)$ , is:

$$\langle \nu^2 \rangle_F = \int F(\nu)(\nu - \nu_c)^2 d\nu \quad (\text{A7})$$

The broadening is then seen to be the difference between the measured widths of the peaks from the strain free regions and from the stressed regions:

$$\begin{aligned} \langle \nu^2 \rangle_F - \langle \nu^2 \rangle_0 &= \int \Delta\nu^2 W(\Delta\nu)d\Delta\nu - \overline{\Delta\nu}^2 \\ &= \langle \Delta\nu^2 \rangle \end{aligned} \quad (\text{A8})$$

Again, the measured broadening and the stress distribution is related by the weighting function.

## B Polycrystalline Averages of Direction Cosines

Collected here for convenience are the polycrystalline averages of the direction cosines  $a_{ij}$ , appearing in tensor transformation relations of the form:

$$\sigma'_{ij} = a_{im} a_{jn} \sigma_{mn} \quad (\text{B1})$$

In terms of the usual Euler angles  $(\theta, \phi, \psi)$ , the transformation matrix is

$$a_{ij} = \begin{pmatrix} \cos \phi \cos \psi - \sin \phi \cos \theta \sin \psi & -\cos \phi \sin \psi - \sin \phi \cos \theta \cos \psi & \sin \theta \sin \phi \\ \sin \phi \cos \psi + \cos \phi \cos \theta \sin \psi & -\sin \phi \sin \psi + \cos \phi \cos \theta \cos \psi & -\sin \theta \cos \phi \\ \sin \theta \sin \psi & \sin \theta \cos \psi & \cos \theta \end{pmatrix}$$

where

$$0 \leq \phi \leq 2\pi, \quad 0 \leq \theta \leq \pi, \quad 0 \leq \psi \leq 2\pi \quad (\text{B2})$$

If, as in a polycrystalline material, the orientations of the grains are at random, the probability a grain director is oriented at  $(\theta, \phi, \psi)$  is given by

$$P(\theta, \phi, \psi) = \frac{1}{8\pi^2} \sin \theta d\theta d\phi d\psi \quad (\text{B3})$$

By averaging over all possible angles, the following relations used to derive equation 7 and 8 are obtained:

$$\overline{a_{ij}^2} = \frac{1}{3}; \quad \overline{a_{ij} a_{ik}} = 0, \quad j \neq k;$$

$$\overline{a_{ij}^4} = \frac{1}{5}; \quad \overline{a_{ij}^2 a_{ik}^2} = \frac{1}{15}, \quad j \neq k; \quad \overline{a_{ij}^2 a_{lk}^2} = \frac{2}{15}, \quad i \neq l, j \neq k;$$

$$\overline{a_{21}^3 a_{22} a_{23}} = \overline{a_{21} a_{22}^2 a_{23}} = \overline{a_{21} a_{22} a_{23}^2} = 0;$$

and

$$\overline{a_{21} a_{22} a_{31} a_{32}} = \overline{a_{21} a_{23} a_{31} a_{33}} = \overline{a_{22} a_{23} a_{32} a_{33}} = -\frac{1}{15}.$$

## REFERENCES

1. P. Zorabedian and F. Adar, "Measurement of Local Stress in Laser Recrystallized Lateral Epitaxial Silicon Films Over Silicon Dioxide Using Raman Scattering", *Applied Physics Letters*, **43** [2] 177-179 (1983).
2. L. Grabner, "Spectroscopic Technique for the Measurement of Residual Stress in Sintered  $\text{Al}_2\text{O}_3$ ", *Journal of Applied Physics*, **49** [2] 580-583 (1978).
3. R. A. Forman, G. J. Piermarini, J. D. Barnett and S. Block, "Pressure Measurement Made by the Utilization of Ruby Sharp Line Luminescence", *Science*, **176** 284-285 (1972).
4. A.L. Schawlow, "Fine Structure and Properties of Chromium Fluorescence in Aluminum and Magnesium Oxide", pp 50-64 in *Advances in Quantum Electronics*. Edited by J.R. Singer, Columbia University Press, New York, 1961.
5. S. Sugano and Y. Tanabe, "Absorption Spectra of  $\text{Cr}^{3+}$  in  $\text{Al}_2\text{O}_3$ ", *Journal of the Physical Society of Japan*, **13** [8] 880-910 (1958).
6. S. E. Molis and D. R. Clarke, "Measurement of Stresses Using Fluorescence in an Optical Microprobe: Stresses Around Indentations in a Chromium-Doped Sapphire", *Journal of the American Ceramic Society*, **73** [11] 3189-3194 (1990).
7. A.L. Schawlow, A. H. Piksis and S. Sugano, "Strain Induced Effects on the Degenerate Spectral Line of Chromium in  $\text{MgO}$  Crystals", *Physical Review*, **122** [5] 1469-1477 (1961).
8. Jun He, Qing Ma and D.R. Clarke, to be published.
9. D. R. Clarke and F. Adar, "Measurement of the Crystallographically Transformed Zone Produced by Fracture in Ceramics Containing Tetragonal Zirconia", *Journal of the American Ceramic Society*, **65** [6] 284-288 (1982).
10. F. Adar and D.R. Clarke, "Raman Microprobe Spectroscopy of Ceramics", pp 307-310 in *Microbeam Analysis*. Edited by K.F.J. Heinrich, San Francisco Press, San Francisco,

1982.

11. S.L. Wunder and P.E. Schoen, "Pressure Measurement at High Temperatures in the Diamond Anvil Cell", *Journal of Applied Physics*, **52** [6] 3772-3775 (1981).
12. R.G. Munro, G.J. Piermarini, S. Block and W.B. Holzapfel, "Model Line-Shape Analysis for the Ruby R Lines Used for Pressure Measurement", *Journal of Applied Physics*, **57** [2] 165-169 (1985).
13. E. Feher and M.D. Sturge, "Effect of Stress on the Trigonal Splittings of  $d^3$  Ions in Sapphire ( $\alpha$ - $\text{Al}_2\text{O}_3$ )", *Physical Review*, **172** [2], 244-249 (1968).
14. Qing Ma and D. R. Clarke, to be published.
15. J. E. Blendell and R. L. Coble, "Measurement of Stress Due to Thermal Expansion Anisotropy in  $\text{Al}_2\text{O}_3$ ", *Journal of the American Ceramic Society*, **65** (3) 174-178 (1982).

## FIGURE CAPTIONS

1. Schematic diagram of a representative grain cut by an arbitrary dividing plane ( $z = 0$ ) through a polycrystalline material, illustrating the coordinates and angles used in the text in describing the orientation of the grain.
2. Measured peak shifts of the  $R_1$  (top) and  $R_2$  (bottom) fluorescence lines from a polycrystalline alumina sample as a function of applied stress. The sample was loaded under four-point bending and spectra were recorded from different positions on both the tensile and compressional sides and over the stress range indicated. The solid line through the data points represents the line of best-fit. Its slope is, within experimental uncertainty, the same as that predicted using equation 7.
3. Measured peak broadening of the  $R_1$  and  $R_2$  fluorescence lines as a function of stress. The broadening was obtained from the same spectra as were used to make the measurements in figure 2.
4. Peak shift of the  $R_1$  and  $R_2$  fluorescence lines as a function of applied stress for a sapphire crystal containing a surface stressed layer. The solid line is the line of best fit to the data. The surface stress was produced by in-diffusion of chromium. Details are given in the text.
5. A comparison of the  $R_1$  and  $R_2$  fluorescence lines from sapphire and a polycrystalline alumina (Coors AD995). The broadening of the lines from the polycrystalline alumina is a result of the distribution of residual thermal expansion anisotropy stresses within the material. Both materials contain a trace of chromium impurity, sufficient to cause fluorescence.

TABLE I

SAMPLE	$\overline{\Delta\nu}$	$\overline{\sigma}_a$	$\overline{\sigma}_c$	$\sqrt{\langle \Delta\nu^2 \rangle}$	$\sigma_w$
	cm <sup>-1</sup>	MPa	MPa	cm <sup>-1</sup>	MPa
AD96	-0.21	-190	380	2.5	430
AD995	-0.15	-135	270	3.6	620
UCSB1	-0.15	-135	270	1.9	330
UCSB2	-0.23	-210	420	1.4	240

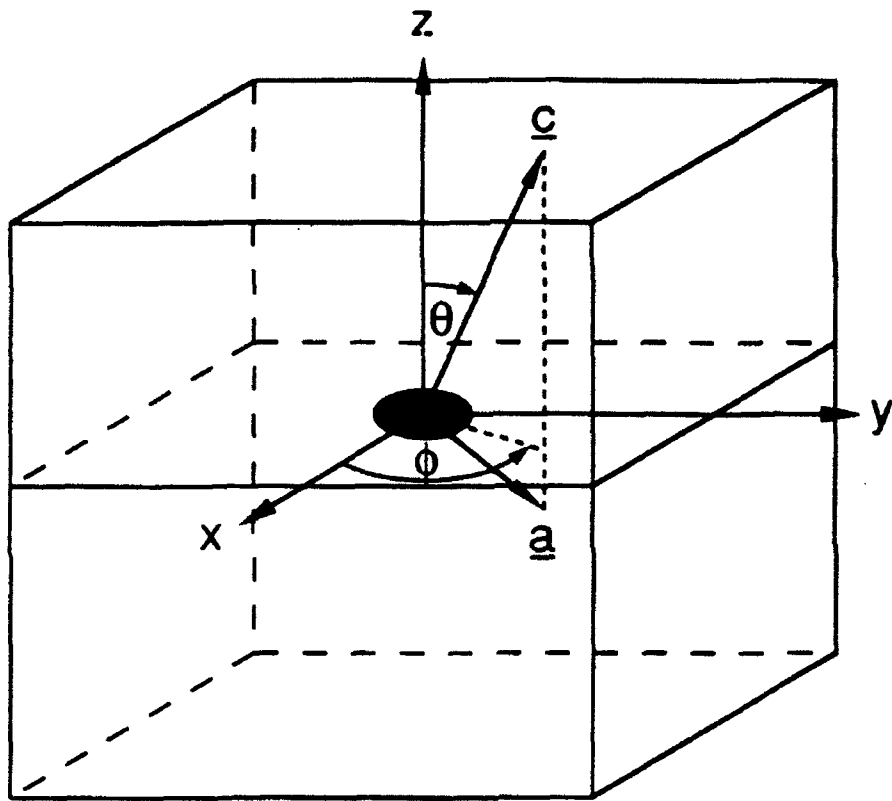


Fig. 1

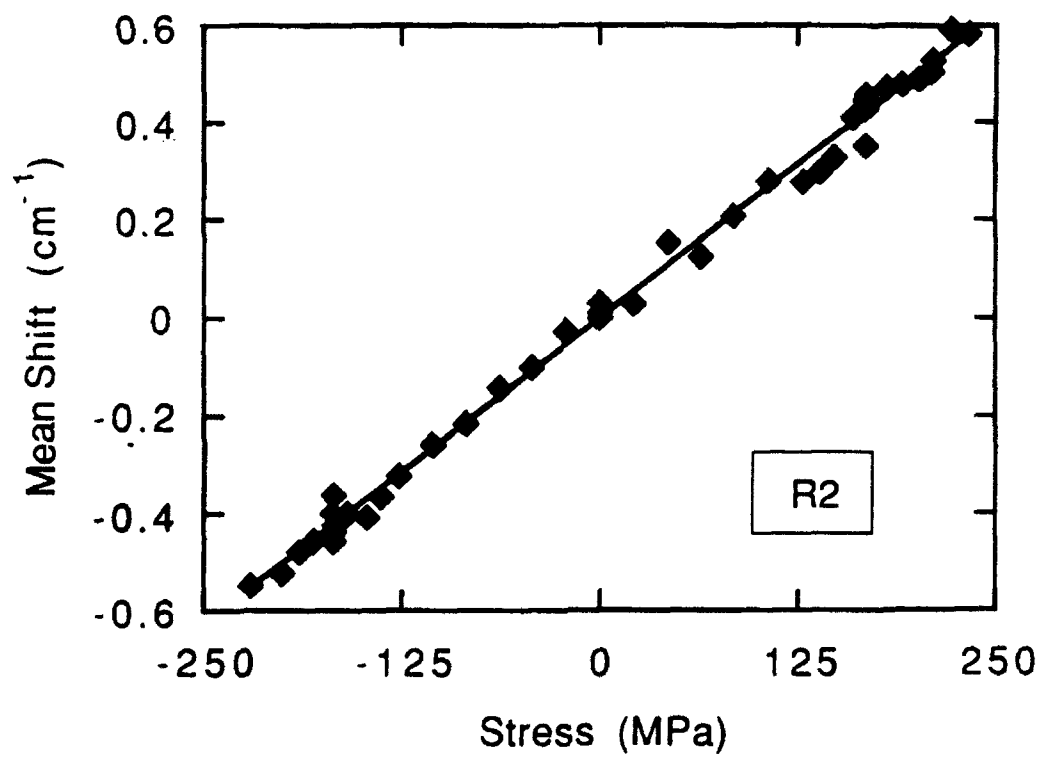
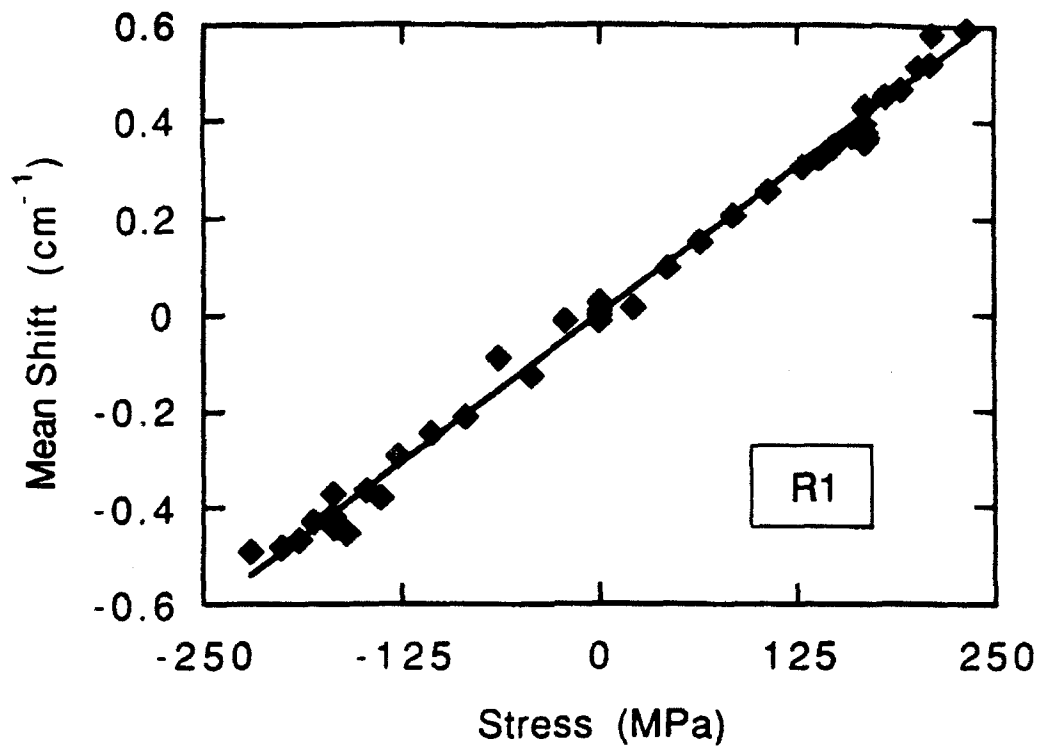


Fig. 2

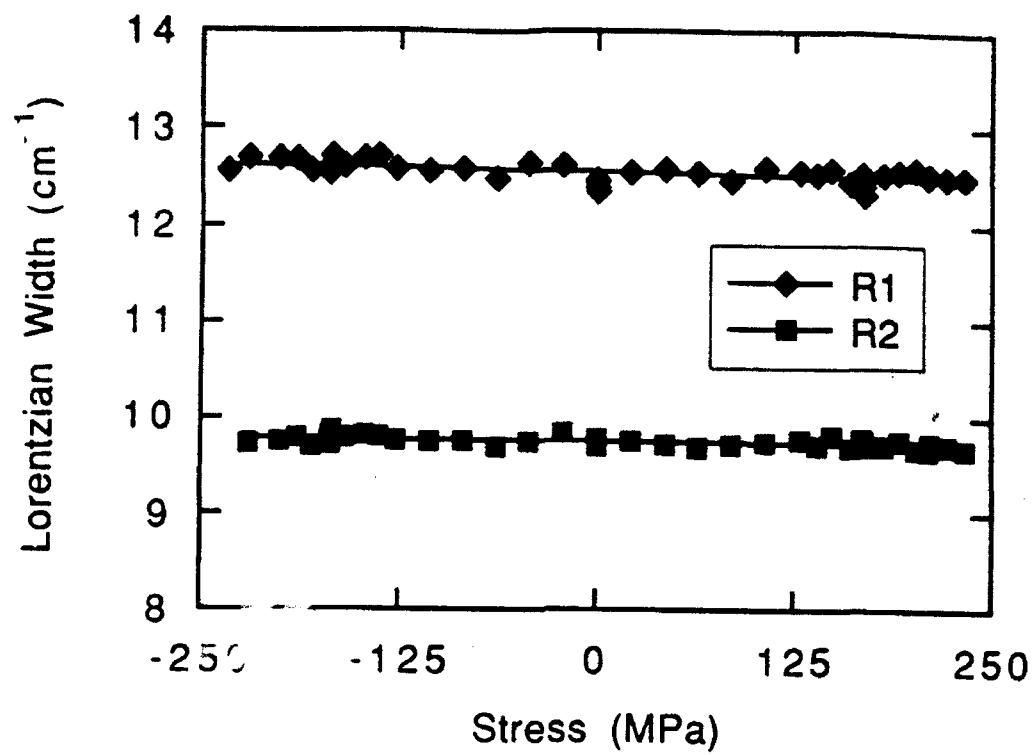


Fig. 3

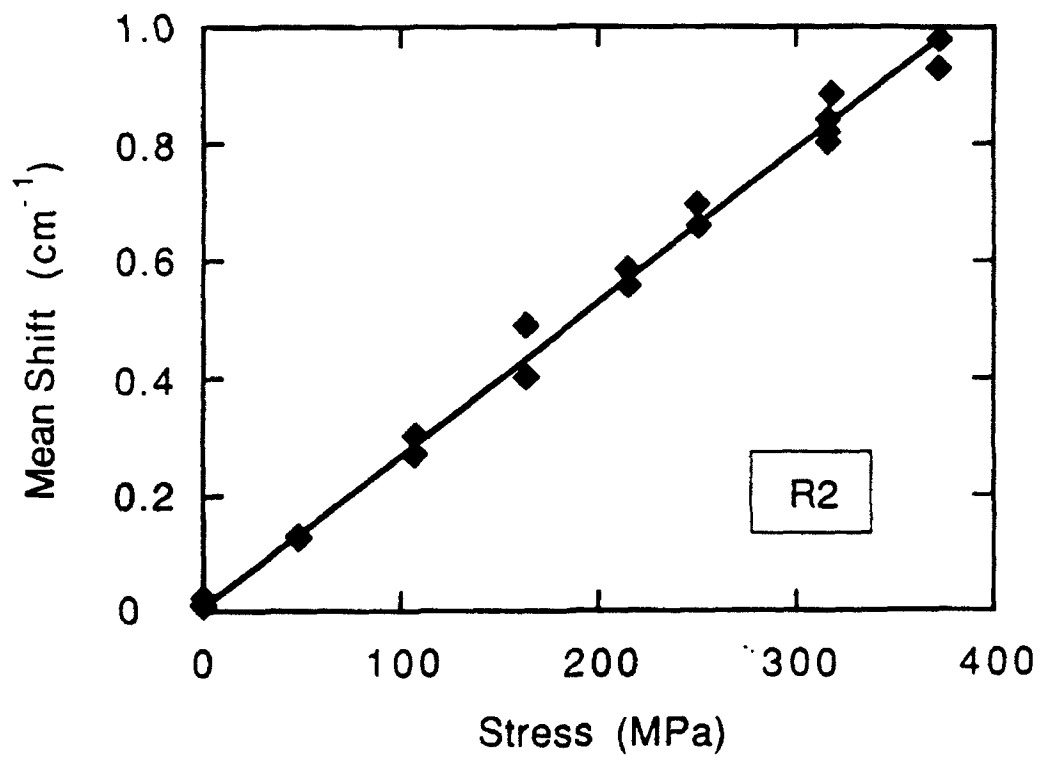
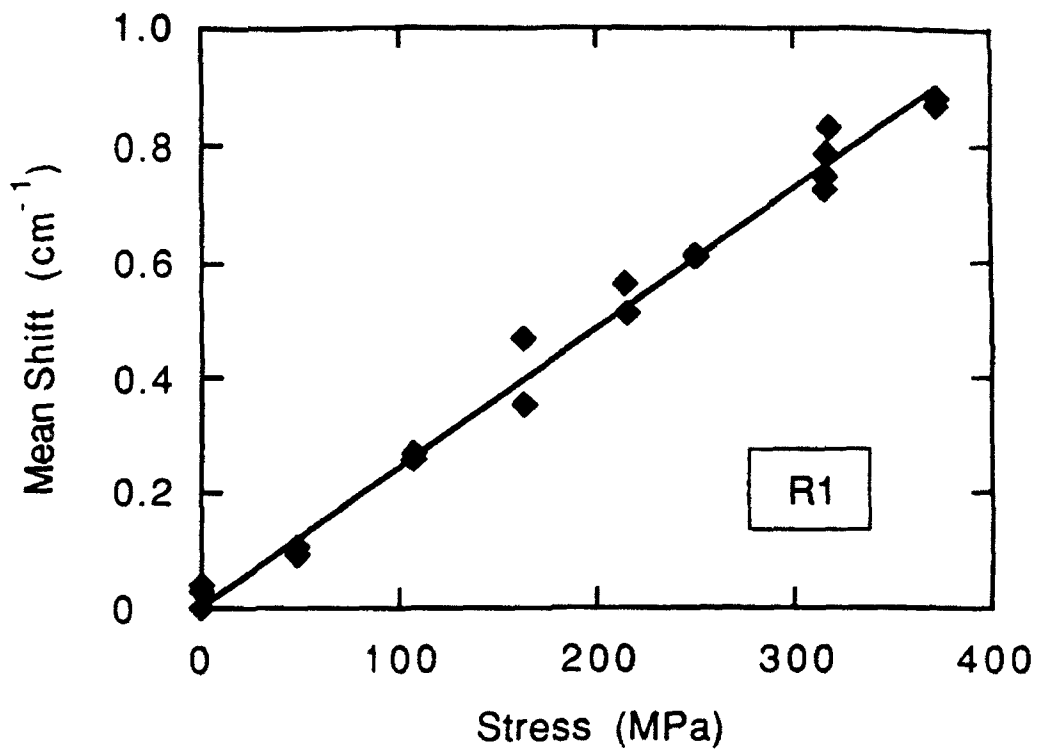


Fig. 4

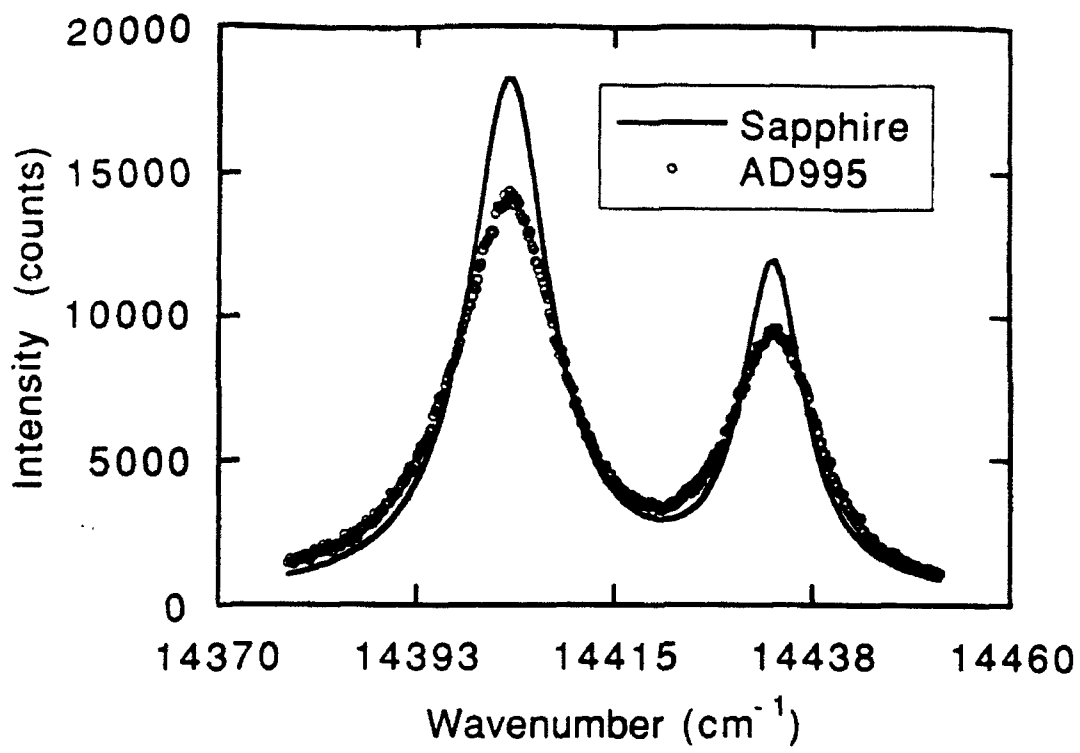


Fig. 5

**MATERIALS UCSB**



**Measurement of Residual Stresses in Sapphire  
Fiber Composites Using Optical Fluorescence.**

by

**Qing Ma and David R. Clarke  
Materials Department  
University of California, Santa Barbara**

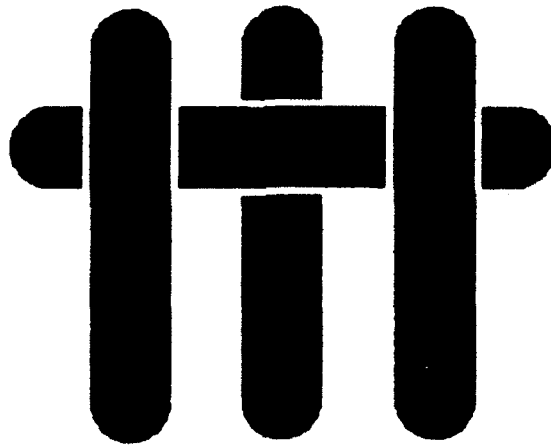
**A Technical Report for**

**Office of Naval Research**

**Contract No. N00014-91-J-1875**

**Principal Investigator: David R. Clarke  
Materials Department  
University of California  
Santa Barbara, CA 93106**

MATERIALS UCSB



MEASUREMENT OF RESIDUAL STRESSES  
IN SAPPHIRE FIBER COMPOSITES  
USING OPTICAL FLUORESCENCE

Qing Ma and David R. Clarke

Materials Department  
University of California  
Santa Barbara, California 93106

**Abstract**

The residual stresses in c-axis sapphire fibers in a  $\gamma$ -TiAl matrix and in a polycrystalline  $\text{Al}_2\text{O}_3$  matrix as a function of distance below a surface are determined. They are obtained from the shift in frequency of the characteristic R2 fluorescence line of chromium in sapphire obtained by focussing an optical probe at different depths in a sapphire fiber intersecting the surface of the composite. The method is described together with its calibration. Both the axial and radial components of the residual stress in the fiber are observed to vary over a depth of approximately the fiber diameter and are then almost independent of depth.

## 1 Introduction

When a composite material is cooled down from its fabrication temperature, thermal mismatch residual stresses develop, which can have a profound influence on the mechanical properties of the composite. For example, in many ceramic fiber reinforced metal matrix or glass matrix composites the thermal expansion coefficient of the matrix  $\alpha_m$  is considerably larger than that of the fiber  $\alpha_f$  and so large compressive stresses can develop in the fiber. The axial compressive stress creates a large stress difference between debonded and bonded regions of the interface when the material is under applied tension, facilitating interfacial crack growth [1,2], a pre-requisite for fiber pull-out. On the other hand, the large radial compressive stress produces large friction forces in the debonded region, which retards fiber sliding and consequently shortens fiber pull-out length [2,3]. It is therefore possible to optimize the mechanical properties of such composites by tailoring the residual stresses through appropriate processing conditions and the use of interfacial coatings [4].

Unfortunately, accurate information about the residual stresses in embedded fibers is usually unavailable since their measurement is particularly difficult. As a result, estimations based on the thermal and elastic properties of the individual material components are usually used in various analyses. This approach requires accurate knowledge of the effective temperature change  $\Delta T$ , which is usually an unmeasurable quantity, and is difficult to estimate without detailed knowledge of the stress relaxation mechanisms, especially near the interface. Furthermore, such estimates can not take into account the variations from fiber to fiber due to irregularities in coatings and interfacial roughness: details which are important in understanding individual fiber pull-out/push-out tests. Direct measurement of the residual stresses in fibers is, in principle, possible by a variety of diffraction techniques. For

instance, X-ray diffraction using ultra-fine beams can provide strain information of individual fibers. However, it suffers from having a relatively small penetration depth ( $\sim 50 \mu\text{m}$ ) [5,6] and can therefore only measure stresses near the surface, which could be significantly different from those deeper inside the composite. Neutron scattering, whilst capable of probing fiber stresses throughout the composite [7,8], has insufficient spatial resolution to study individual fibers or to ascertain stress distributions along the fibers.

An alternative method of measuring stresses in fibers is by using piezo-spectroscopic effects. The basis of such methods is that the characteristic luminescence lines (Raman or fluorescence) of the material shift with stress. By utilizing an optical microscope to define a probe, it is relatively easy to select regions of interest with spatial resolution of only a few microns [9] either on the surface of a composite, or if the matrix is transparent, within the composite. For example, in the case of polydiacetylene fibers embedded in an optically transparent epoxy [10], Raman spectra were collected from different positions along a fiber to obtain the stress distribution along it. Since optical spectrum can be collected and analyzed with relative ease compared to most diffraction methods, such measurements can be performed routinely.

In this paper, we present a new method of measuring residual stresses in embedded transparent fibers, one that utilizes optical fluorescence, and illustrate its application to determining the residual stresses in sapphire fibers in  $\gamma\text{-TiAl}$  and  $\text{Al}_2\text{O}_3$  matrices. The theoretical basis of the fluorescence method was described in detail in an earlier work [11]. Briefly, the frequency shift of a characteristic fluorescence line is stress dependent and is given by:

$$\Delta\nu = \Pi_{ij} \sigma_{ij}^* \quad (1)$$

where  $\Pi_{ij}$  are the piezo-spectroscopic coefficients relating frequency shift to stress, and  $\sigma_{ij}$  is the stress tensor represented in the crystallographic frame of reference.

The method is to use an optical microscope to focus a light beam on the end of an exposed sapphire fiber (figure 1), measure the frequency shift of a characteristic luminescence line and then repeat the measurement at successively deeper points of focus into the fiber. Using the lenses of the microscope to form an optical probe enables the luminescence to be collected, for any particular point of focus, from a relatively small depth of field. This facilitates high spatial resolution [12,13] along the fiber but at the same time means that the observed frequency shifts have to be deconvoluted using a previously established calibration of the microscope convolution function (the depth of field function). This is described in the following section. Also described is a test of the accuracy of the stress profiling method in which the stress through the thickness of a ruby beam under four-point loading is measured and compared with the known elastic solution.

To illustrate the application of the technique we have measured the residual stresses in Saphikon sapphire fibers. They have sufficient levels of chromium impurity to produce sufficiently intense fluorescence lines  $R_1$  and  $R_2$  of ruby when excited by an argon ion laser. Because the fibers are single crystal with their  $c$ -axis along the fiber axis, the residual stresses inside the fibers are expected to have cylindrical symmetry. As a result, there are only two independent stress components, the radial component  $\sigma_r$  and the axial component  $\sigma_z$ . This simplifies equation 1 to be:

$$\Delta\nu = 2\Pi_a \sigma_r + \Pi_c \sigma_z \quad (2)$$

where  $\Pi_a$  and  $\Pi_c$  are the piezo-spectroscopy coefficients for the  $a$  and  $c$  directions. They have been measured to have values of 2.70 and 2.15  $\text{cm}^{-1}\text{GPa}^{-1}$ , respectively [14]. A positive

shift implies tension and a negative one implies compression. In section 3, measurements of line shifts along fibers in both  $\gamma$ -TiAl and  $\text{Al}_2\text{O}_3$  matrices as a function of depth are made. Since the frequency shifts are dependent on both the axial and radial stress components, their separation requires the solution of the appropriate elastic equations. This is described, using the results of a finite element computation in section 4. From this, the stresses as a function of depth are determined.

## 2 The Through-Focus Depth Profiling Method <sup>1</sup>

### 2.1 Depth of Field Function

The depth resolution of the optical microprobe used for the fluorescence measurements is determined by the numerical aperture of the objective lens and the size of the collection aperture used [12,13]. As illustrated in figure 2, when the excitation laser is focused at a distance  $z$  below the top surface of a transparent material with uniform concentration of fluorescing species, only the signal generated in a small volume above and below the focal plane is collected. The total signal collected is then the integral of the fluorescence from different depths:

$$I(z) = \int_{-z}^{t-z} \gamma(u) du \quad (3)$$

where  $g(u)$  is the depth of field function of the lens used to describe the relative collection efficiency as a function of  $u$ , the distance from the focal plane.

By moving the focal plane from a position above the top surface to a position below the surface of a thick sapphire disk ( $t \rightarrow \infty$ ) containing adequate chromium concentration.

---

<sup>1</sup> The general procedures for optical fluorescence measurement and analysis were described in detail in [11] and therefore not included in this work.

and recording the fluorescence line intensity as a function of depth  $z$ , the depth resolution function  $g$  is obtained from equation 3, namely:

$$g(z) = \frac{dI(z)}{dz} \quad (4)$$

The depth resolution function for our optical microprobe using a 50/0.55 objective lens and a 200  $\mu\text{m}$  collection aperture was measured using the above method and is shown in figure 3. As can be seen, the collection efficiency is maximum at the focal plane, and decrease rapidly with distance on either side of the focal plane.

## 2.2 Measurement of the Frequency Shift Depth Profile

We now suppose that there exists a stress field that only varies with depth  $z$ . From equation 2, the shift of a fluorescence line associated with the increment in signal from a narrow slice of material at depth  $z + u$  is

$$\Delta\nu(z + u) = 2\Pi_a \sigma_r(z + u) + \Pi_c \sigma_z(z + u) \quad (5)$$

The measured shift with focal point positioned at depth  $z$  is then a weighted average of the signals from all depths:

$$\overline{\Delta\nu(z)} = \frac{\int_{-z}^{t-z} \Delta\nu(z + u) g(u) du}{\int_{-z}^{t-z} g(u) du} \quad (6)$$

Provided the depth of field function  $g(z)$  is known, the real depth profile  $\Delta\nu(z)$  can be deconvoluted from equation 6.

To establish that the foregoing methodology is correct, the stress field through the thickness of a dilute ruby beam in 4-point loading was measured and compared with the elastic solution for the stress. A number of fluorescence spectra were taken as the laser beam was

focused at different depths from the top, tension surface to the bottom, compression surface of the beam. The measured shifts are plotted in figure 4 as the solid dots. The deconvoluted data is shown by the solid line. The deconvolution was obtained by assuming that the real shift  $\Delta\nu(z)$  is a linear function of depth  $a + bz$  since it is known that the stress distribution varies linearly with the depth  $z$  for a rectangular beam under 4-point loading. This function is then convoluted with the depth of field function  $g(z)$ . By fitting the resulting convoluted function to the measured shifts, the coefficients  $a$  and  $b$  are obtained. The initially assumed function, with the coefficients obtained by fitting, is then regarded as the deconvoluted shift  $\Delta\nu(z)$  directly related to the stress distributions by equation 2. The straight solid line in figure 4 therefore represents the real shifts. As expected, and required, the zero shift position coincides with the neutral plane of the beam. The stress distribution calculated by using equation 2 is also in good agreement with that obtained from beam theory and loading conditions. As a further check, the convoluted shift, obtained by convoluting the derived values of the real shift with the instrument function  $g(z)$  is shown by the dashed curve. It has excellent fit with the measured data except for the slight deviation near the compression surface which, we believe, is due to the fact that the focus deteriorates after light has passed all the way through the ruby beam. These observations thus confirm that the through-focus method can indeed accurately measure the depth profile of the stresses.

### 3 Measured Frequency Shifts From Embedded Sapphire Fibers

The depth profiling method has been applied to two different sapphire fiber composites: the first, a  $\gamma$ -TiAl matrix composite with carbon black/alumina double fiber coatings on the sapphire fibers and, the second, a polycrystalline  $\text{Al}_2\text{O}_3$  matrix with a thin molybdenum

coating on the fibers. In each case, the fiber diameter is about 120  $\mu\text{m}$ . Thin slices of composite with parallel surfaces perpendicular to the sapphire fibers were cut to about 450  $\mu\text{m}$  and 600  $\mu\text{m}$  thick for the  $\gamma$ -TiAl matrix and the  $\text{Al}_2\text{O}_3$  matrix composites respectively. The top surface of the specimens were then polished to obtain an optical finish at the fiber ends.

The measured and the deconvoluted frequency shift as a function of depth into a sapphire fiber in  $\gamma$ -TiAl matrix, as well as the convoluted function are plotted in figure 5. Since  $\gamma$ -TiAl has considerably larger thermal expansion coefficient than sapphire (table 1), the residual stress developed by thermal mismatch in the fiber should be compressive in both radial and axial directions. This is consistent with the large negative shifts observed when the probe is focused deep in the interior of the specimen. Near the surface, the axial stress approaches zero as required by force balance. The deconvoluted shift becomes positive near the surface indicating that the radial stress becomes tensile near the surface. In the case of the sapphire fibers in polycrystalline  $\text{Al}_2\text{O}_3$ , the residual stress is mainly caused by the anisotropy of the thermal expansion coefficient of sapphire. As show in figure 6, the relatively large negative shifts near the surface indicate that the radial stress near the surface is compressive, since the axial stress must approach zero due to force balance requirement, and thus does not contribute to the shift. The magnitude of the negative shift becomes progressively smaller with increasing of depth implying that the negative shift associated with the radial compressive stress is partially compensated by the positive shift resulting from the build up of the axial tensile stress. These observations are consistent with the fact that the thermal expansion coefficient of polycrystalline  $\text{Al}_2\text{O}_3$  is larger than that of the sapphire in the  $a$ -direction, but smaller than that in the  $c$ -direction. A notable feature of the depth profile of the shift, in both systems, is the near exponential dependence. This

is indicative of the fibers being fully bonded to the matrices and the fiber/matrix systems being elastic.

#### 4 Analysis

The residual stresses in the sapphire fibers are related to the observed frequency shifts presented in the previous section by equation 2. In order to obtain actual values of the two stress components, an additional relationship between the two components is evidently required. Two difficulties are associated with establishing such a relationship. First, the residual stresses originate from thermal expansion mismatch but the temperature on cooling at which stress relaxation no longer is effective, and stresses begin to build up, is not known. Secondly, existing equations relating the residual stresses in a fiber embedded in an infinite matrix [2] to the thermal mismatch strain  $\Delta\alpha\Delta T$  are unfortunately not valid for the thin specimens used in this work. Furthermore, rigorous analytical solutions for the residual stress field are not available and the approximate models used in analyzing stresses in fibers, e.g. those in analyzing fiber pull-out/push-out tests [15-17] breakdown near the fiber end. We have therefore had to resort to finite element calculations of the residual stress field for the sapphire/ $\gamma$ -TiAl and sapphire/ $\text{Al}_2\text{O}_3$  systems and use an iterative, self consistent procedure to calculate the residual stresses and the temperature at which the stresses become frozen in. This is described in the following paragraphs. First, however, it should be noted that the stresses can be *estimated* directly from equation 2. For the  $\gamma$ -TiAl matrix system, the residual stresses in the fiber are expected to be compressive. If it is assumed that the magnitude of the radial component is similar to the axial component in the interior of the

composite, then using the shift from deep in the fiber we have from equation 2

$$\sigma_r^{int} \sim \sigma_z^{int} \sim \frac{\Delta\nu^{int}}{2\Pi_a + \Pi_c} \sim 500 \text{ MPa}$$

For the  $\text{Al}_2\text{O}_3$  matrix system, due to the anisotropy of the thermal expansion coefficient of sapphire, the fiber should be under axial tension and radial compression. If we assume that the radial compression stress is about the same in the interior and near the surface, we again can estimate that

$$\sigma_r^{int} \sim \sigma_r^{sur} \sim \frac{\Delta\nu^{sur}}{2\Pi_a} \sim -100 \text{ MPa}$$

and

$$\sigma_z^{int} \sim \frac{\Delta\nu^{int} - 2\Pi_a\sigma_r^{int}}{\Pi_c} \sim 200 \text{ MPa}$$

Quantitative stress distributions can be obtained by comparing in detail the measured shifts with those calculated from the elastic field in the fiber/matrix system. Since the fiber coatings are relatively thin in both composites, we expect their effects on the elastic field to be negligible compared to those of the fiber and matrix. Therefore, in the calculations, the elastic system is simplified as consisting solely of an isotropic matrix of modulus  $E_m$  and Poisson's ratio  $\nu_m$  and a fiber of modulus  $E_f$  and Poisson's ratio  $\nu_f$  (Table 1). The specimen was represented by a thin disk of the same thickness as the corresponding specimen with one cylindrical fiber sitting at the symmetry axis. The diameter of the disk was chosen to be about ten times that of the fiber in order to be consistent with the low fiber volume fraction of both composite systems. The thermal expansion coefficients of the sapphire fiber in both the radial direction  $\alpha_r$  and axial direction  $\alpha_c$  are also listed in Table 1. The mean thermal expansion coefficient for  $\gamma\text{-TiAl}$  is known to be  $11 \sim 13 \times 10^{-6}/^\circ\text{C}$  depending on

the stress frozen-in temperature. However, that of the polycrystalline  $\text{Al}_2\text{O}_3$  is expected to vary from sample to sample depending on the residual matrix porosity. As a result of the complicated stress relaxation processes that occur during cooling, particularly near the interface, the effective thermal expansion coefficient  $\alpha_m$  for both matrices and the effective temperature change  $\Delta T$  were adjusted in the computation to obtain the best agreement with the experimental frequency shift data. The following procedure was adopted. First, reasonable estimates for the matrix thermal expansion coefficient and temperature change  $\alpha_m^{est}$  and  $\Delta T^{est}$  were used in the finite element calculation. The resulting stresses  $\sigma_r^{est}(z)$  and  $\sigma_z^{est}(z)$  were then used in equation 2 to calculate the shift as a function of  $z$ ,  $\Delta\nu_{cal}^{est}(z)$ . This function and the measured shifts are then normalized by their values in the interior of the material:

$$\Delta\nu^{norm} = \frac{\Delta\nu}{\Delta\nu^{int}} \quad (7)$$

By comparing the calculated and measured normalized shifts for a series of values of  $\alpha_m^{est}$ , the value that gives the best agreement is considered as the true  $\alpha_m$ . Then, by requiring that the calculated shift be equal to the measured shift in the interior, the effective temperature difference is proportionally scaled:

$$\Delta T = \Delta T^{est} \frac{\Delta\nu_{meas}^{int}}{\Delta\nu_{cal}^{int}} \quad (8)$$

Finally, the stress distributions are obtained:

$$\begin{aligned} \sigma_r &= \sigma_r^{est} \frac{\Delta T}{\Delta T^{est}} \\ \sigma_z &= \sigma_z^{est} \frac{\Delta T}{\Delta T^{est}} \end{aligned} \quad (9)$$

Since the thermal expansion coefficient of  $\gamma$ -TiAl is considerably larger than  $\alpha_s$  and  $\alpha_c$  of sapphire, the difference between  $\alpha_s$  and  $\alpha_c$  was unimportant. As a result, it was observed that the fitting of the normalized shift was not sensitive to the actual value of  $\alpha_m$ . Figure 7 illustrates the fitting between the measured and the calculated normal shifts for  $\alpha_m = 12$ . The effective temperature drop  $\Delta T$  calculated from equation 8 is  $\sim 750^\circ\text{C}$ , which agrees with  $\alpha_m$ - $T$  curve for  $\gamma$ -TiAl [18]. This temperature change is about  $300^\circ\text{C}$  smaller than the difference between the processing temperature and the room temperature indicating significant stress relaxation occurring during cooling. The stress distributions along the fiber calculated from equation 9 are plotted in figure 8. The axial stress approaches zero as expected and the radial component is positive at the surface as was indicated by the frequency shift measurement. The differences between the calculated and the measured normalized shifts as shown in figure 7 are due to the simplifications used in the model, e.g., neglecting the effects of coatings and assuming perfect interfacial bonding. However, the finite element calculations shows that the stress distributions in the interior of the specimen are not sensitive to small changes in the value of the elastic modulus and the thermal expansion coefficient of the matrix. This is because the values of the stresses are bounded by the measured shifts through equations 2 and scaled by equations 8 and 9. These observations suggest that the stress distributions deduced from the fluorescence data and illustrated in figure 8 are relatively accurate especially in the interior of the specimen. The possibility of some interfacial debonding will be discussed in more detail in the next section.

As expected, the normalized shift calculated for the  $\text{Al}_2\text{O}_3$  matrix system depends much more sensitively on the value of  $\alpha_m$  used in the computation. As show in figure 9,  $\alpha_m = 3.73$  gives the best fit between the calculated and the measured normalized shifts. The effective temperature difference obtained using equation 8 is about  $1300^\circ\text{C}$ , which is about  $200^\circ\text{C}$

lower than the processing temperature again as indication of stress relaxation occurring during cooling. The stress distributions in the sapphire fiber are plotted in figure 10. The observation that the calculated stress distributions in the interior are not sensitive to changes of  $E_m$  also applies in this system. The values of stress in the interior differ less than 5% for the three  $\alpha_m$ 's shown in figure 9. Since the shape of the shift profile depends sensitively to the change of  $\alpha_m$ , the fitting in figure 9 also provides means of estimating the local thermal expansion coefficient of the  $\text{Al}_2\text{O}_3$  matrix, which could be different from the average value of the whole sample because the density of the matrix is slightly lower near the fibers. The resulting value of  $\alpha_m$  can then be used in other analyses, such as for push-out tests.

## 5 Discussion

The analysis in the last section is based on the assumption that the fiber/matrix systems are elastic without any debonding occurring at the interface. This requires that the interfacial shear strength be larger than the maximum interface shear stress. To examine this assumption, the interfacial shear stress is also calculated in the finite element computation. The results corresponding to the best fit conditions determined in the last section are plotted for the sapphire/ $\gamma$ -TiAl and the sapphire/ $\text{Al}_2\text{O}_3$  systems in figure 11. In both systems, the magnitude of the shear stress has a maximum at the surface and decreases to zero with increasing depth. This is expected from the stress distributions in figures 8 and 10 and the force balance requirement:

$$\tau = \frac{R_f}{2} \frac{d\sigma_z}{dz} \quad (10)$$

Whilst the calculated interfacial shear stress for the sapphire/ $\text{Al}_2\text{O}_3$  system is smaller than the interfacial shear strength for the molybdenum/sapphire interface ( $\sim 100 - 300$

MPa) [19] and therefore insufficient to produce any debonding, the shear stress calculated for the sapphire/ $\gamma$ -TiAl system is considerably larger than any reasonable value for the carbon/sapphire interface ( $\sim 100 - 150$  MPa) [4,18]. It is likely that the thin carbon coating on this fiber is not continuous so that the sapphire fiber has direct contact with the polycrystalline  $\text{Al}_2\text{O}_3$  outer coating to form a strongly bonded interface. This has been often observed in the same composite specimen during push-out tests [18]. As mentioned in the last section, the fitting between the calculated and measured frequency shifts near the surface is not perfect. As shown in figure 7, the calculated shift changes more rapidly than that measured within one fiber diameter from the surface. Therefore, the change of the axial stress and consequently the magnitude of the interfacial shear (equation 10) in the real system should be smaller than that calculated. This further suggest that the interface may be debonded for a distance about one fiber diameter from the surface. However, this debonding does not seem to change the stress field significantly, so that the fiber/matrix system still behaves in an elastic manner. This is consistent with the fact that the friction is sufficiently large in this system, due to asperities at the interface [4,20], that the stress distribution is similar to a system with perfect bonding [3]. Therefore, we believe that the residual stresses determined for the sapphire/ $\gamma$ -TiAl system, especially in the interior of the composite, are not significantly affected by possible debonding near the surface.

## 6 Conclusions

By utilizing the optical fluorescence from chromium impurities in sapphire fibers, we have determined the residual stress distributions in embedded fibers in both a  $\gamma$ -TiAl matrix and a polycrystalline  $\text{Al}_2\text{O}_3$  matrix composite. The axial and radial components of the residual

stress, produced by differential thermal contraction on cooling after fabrication, in the fibers are determined as a function of depth below the composite surface. For both composites, the two stress components vary over a distance of about the fiber diameter from the surface and then are almost independent of distance further into the composite.

### ACKNOWLEDGMENT

This work was supported by the Office of Naval Research under grant N00014-91-J-1375 (QM) and the DARPA URI program at UCSB under contract N00014-92-J-1308 (DRC). The authors are grateful to Dr. T.J. Machin and J. Davis, UCSB, for providing the composite samples used in this work.

## References

1. J.W. Hutchinson and H.M. Jensen, *Mech. Materials*, 9, 139 (1990).
2. R.J. Kerans and T.A. Parthasarathy, *J. Am. Ceram. Soc.*, 74, 1585 (1991).
3. K.T. Faber, S.H. Advani, J.K. Lee, and J.T. Jinn, *J. Am. Ceram. Soc.*, 69, C-208 (1986).
4. T.J. Mackin, J.Y. Yang, C.G. Levi and A.G. Evans, submitted to *Mat. Sci. Eng.*
5. P. Predecki, A. Abuhasan, and C.S. Barrett, *Adv. X-ray Anal.*, 31, 231, (1988).
6. A. Abuhasan, C. Balasingh, and P. Predecki, *J. Am. Ceram. Soc.*, 73, 2474 (1990).
7. S. Majumdar, D. Kupperman, and J. Singh, *J. Am. Ceram. Soc.*, 71, 858 (1988).
8. A.J. Allen, M.A.M. Bourke, S. Dawes, M.T. Hutchings and P.J. Withers, *Acta Metall. Mater.*, 40, 2361 (1992).
9. S. E. Molis and D. R. Clarke, *J. Am. Ceram. Soc.*, 73, 3189 (1990).
10. I.M. Robinson, R.J. Young, C. Galotis and D.N. Batchelder, *J. Mater. Sci.*, 22, 3642 (1987).
11. Q. Ma and D. R. Clarke, *J. Am. Ceram. Soc.*, submitted.
12. M. Pluta, *Advanced Light Microscopy 1*, Elsevier, Amsterdam, 1988.
13. F. Adar and D.R. Clarke. "Raman Microprobe Spectroscopy of Ceramics", pp 307-310 in *Microbeam Analysis*. Edited by K.F.J. Heinrich. San Francisco Press, San Francisco, 1982.

14. R.G. Munro, G.J. Piermarini, S. Block and W.B. Holzapfel, *Journal of Applied Physics*, 57, 165 (1985).
15. A. Takaku and R.G.C. Arridge, *J. Phys. D6*, 2038 (1973).
16. D.K. Shetty, *J. Am. Ceram. Soc.*, 71, C-107 (1988).
17. Y.C. Gao, Y.W. Mai, and B. Cotterell, *J. Appl. Math. Phys.*, 39, 550 (1988).
18. T.J. Mackin, private communication.
19. J. Davis and A.G. Evans, to be published.
20. T.J. Mackin, P.D. Warren and A.G. Evans, *Acta Metall. Mater.*, 40, 1251 (1992).

TABLE I

PROPERTY	Sapphire	$\gamma$ -TiAl	Al <sub>2</sub> O <sub>3</sub>
$E$ (GPa)	434	173	250
$\nu$	0.27	0.33	0.27
$\alpha$ (10 <sup>-6</sup> /°C)	3.3 (a), 9.0 (c)	11 ~ 13	3.3 < $\alpha$ < 9.0

## Figure Captions

Figure 1. Schematic diagram of the optical arrangement used to collect fluorescence from a region in an embedded, transparent fiber below its surface. The stress induced shift in frequency of a characteristic luminescence line is used to determine the stress in the probed region.

Figure 2. Illustration of the effect of the finite depth of field of the optical system used. When the excitation laser is focused at a distance  $z$  below the top surface, only the signal generated in a small volume above and below the focal plane is effectively collected.

Figure 3. The depth of field function of the microprobe used. It describes the relative collection efficiency as a function of distance from the focal plane. Details are given in the text.

Figure 4. The fluorescence line shift in the region between the tension surface ( $z = 0$ ) and the compression surface ( $z = 513 \mu\text{m}$ ) of a ruby beam under 4-point bending. The solid line representing the true shift is obtained by deconvoluting the measured shift with the depth of field function.

Figure 5. The line shift depth profiles ( $z = 0$  at the surface) in a  $c$ -axis sapphire fiber embedded in the  $\gamma$ -TiAl matrix.

Figure 6. The line shift depth profiles ( $z = 0$  at the surface) in a  $c$ -axis sapphire fiber embedded in a polycrystalline  $\text{Al}_2\text{O}_3$  matrix.

Figure 7. A comparison of the calculated and the measured normalized shifts as a function of depth for the sapphire/ $\gamma$ -TiAl system.

Figure 8. The radial and axial stresses as a function of depth in the sapphire/ $\gamma$ -TiAl system determined from the fluorescence data.

Figure 9. A comparison of the calculated and the measured normalized shifts as a function of depth for the sapphire/ $\text{Al}_2\text{O}_3$  system.

Figure 10. The radial and axial stresses as a function of depth in the sapphire/ $\text{Al}_2\text{O}_3$  system determined from the fluorescence data.

Figure 11. The interfacial shear stresses in the sapphire/ $\gamma$ -TiAl and the sapphire/ $\text{Al}_2\text{O}_3$  systems calculated from the finite element computation and the fluorescence data.

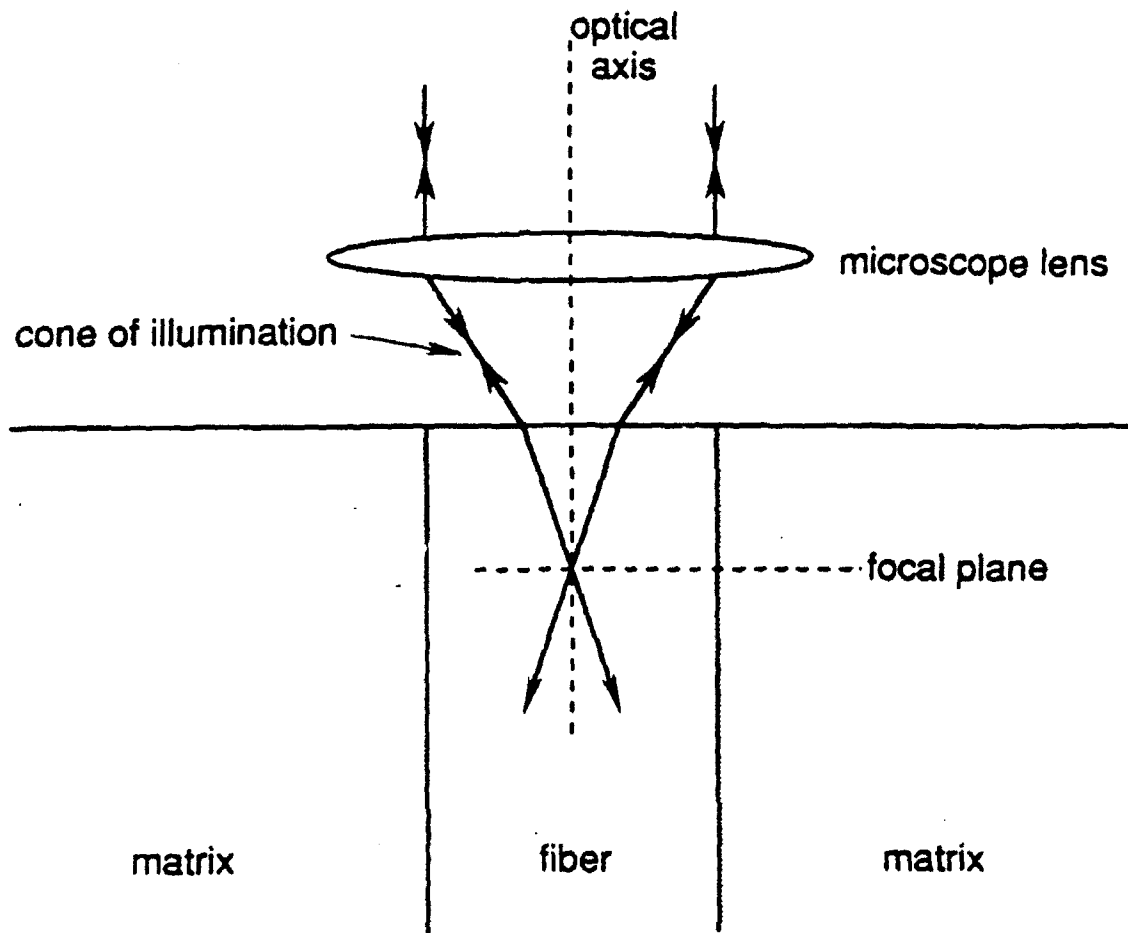


Fig.1

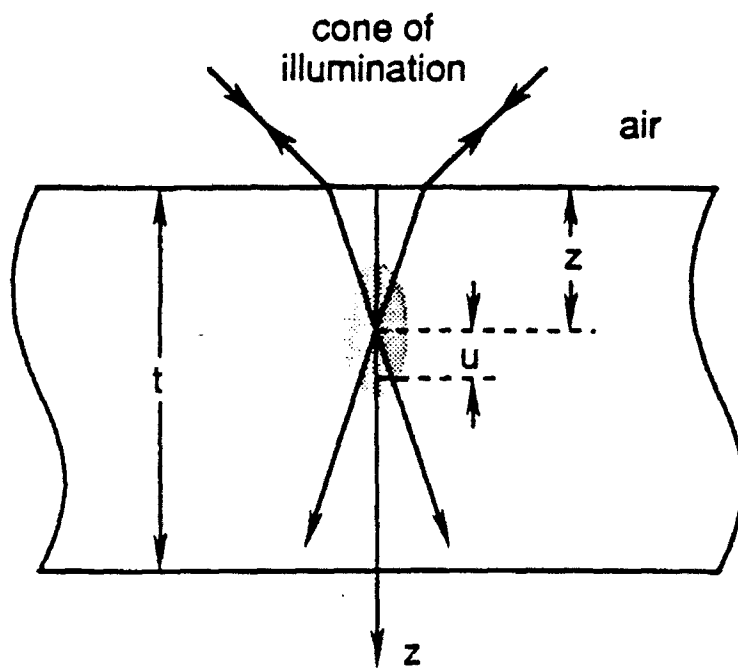


Fig. 2

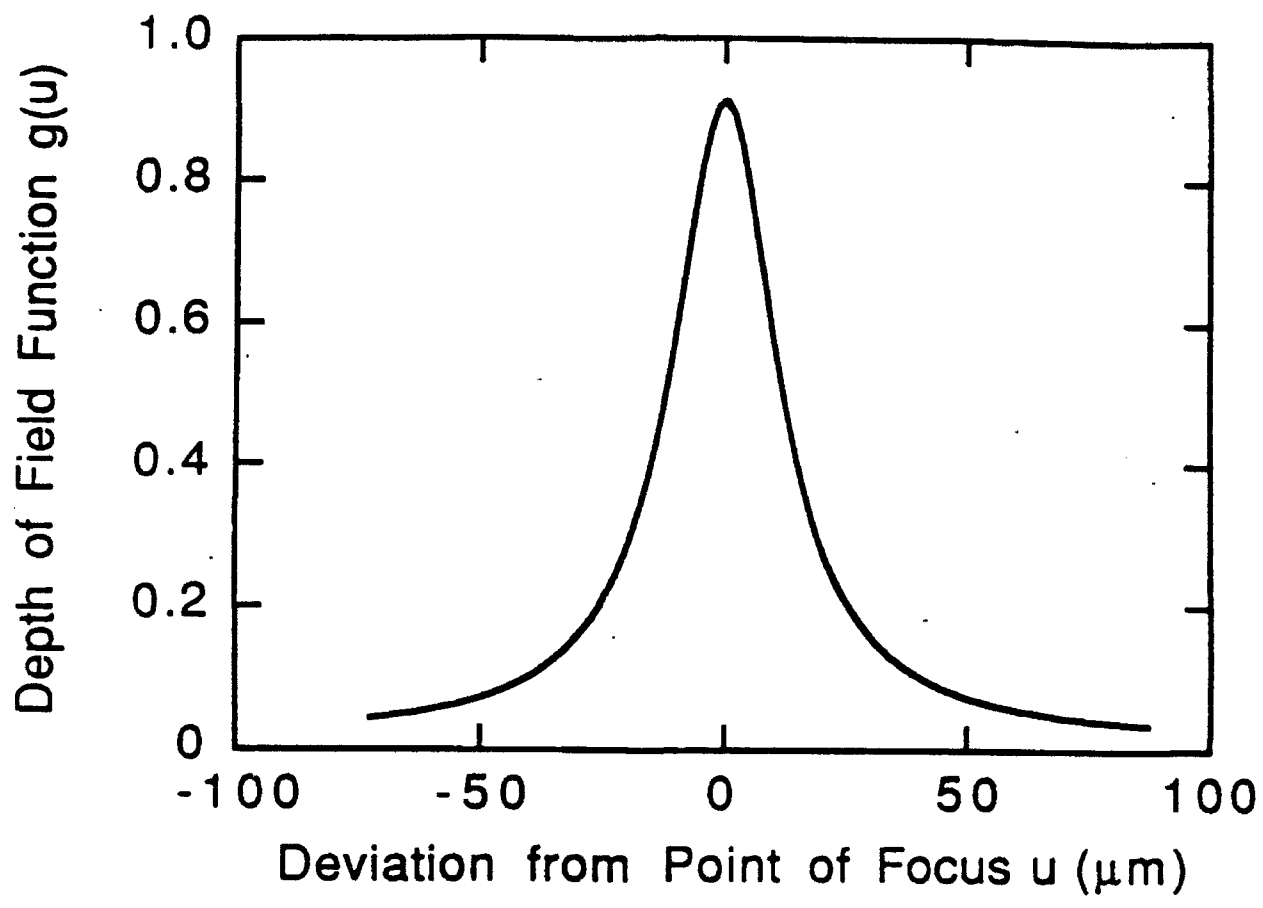


Fig. 3

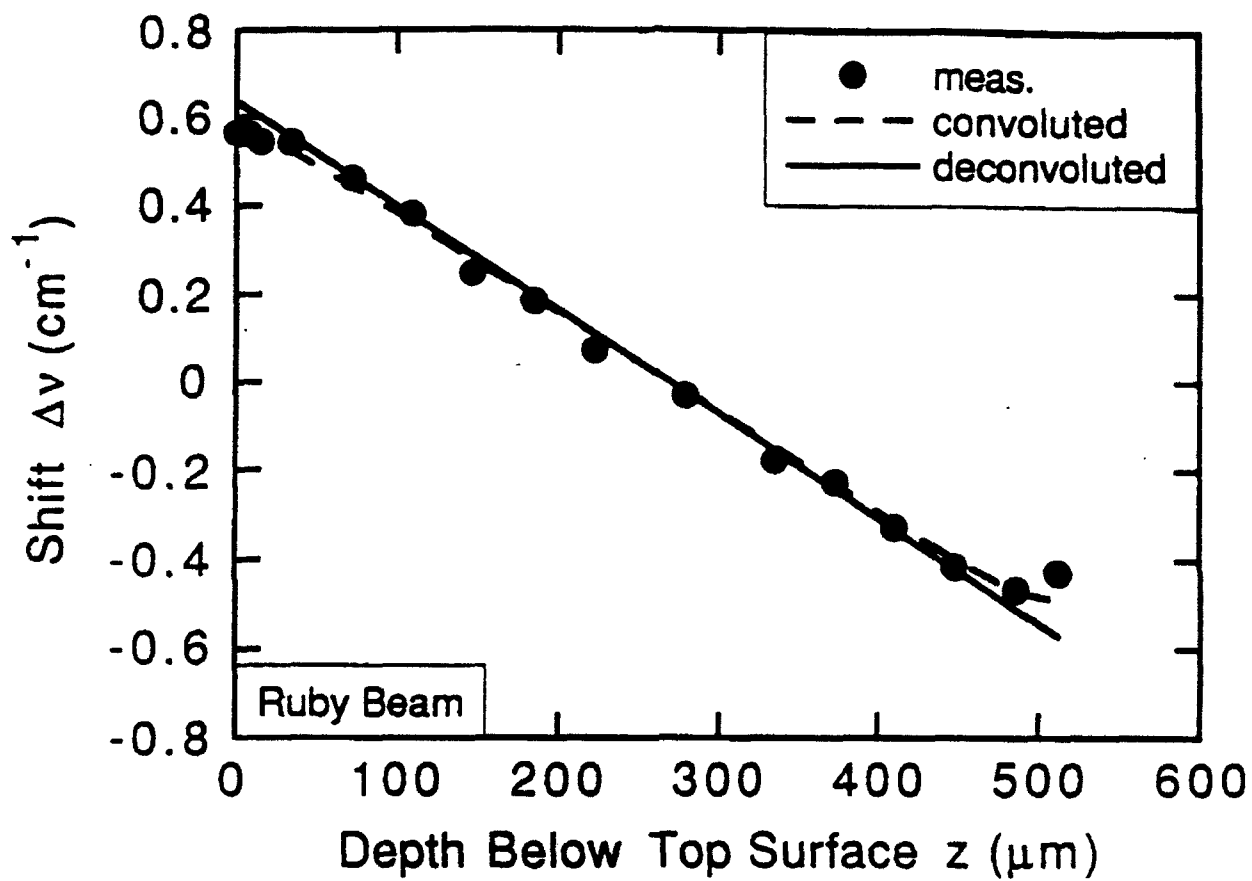


Fig. 4

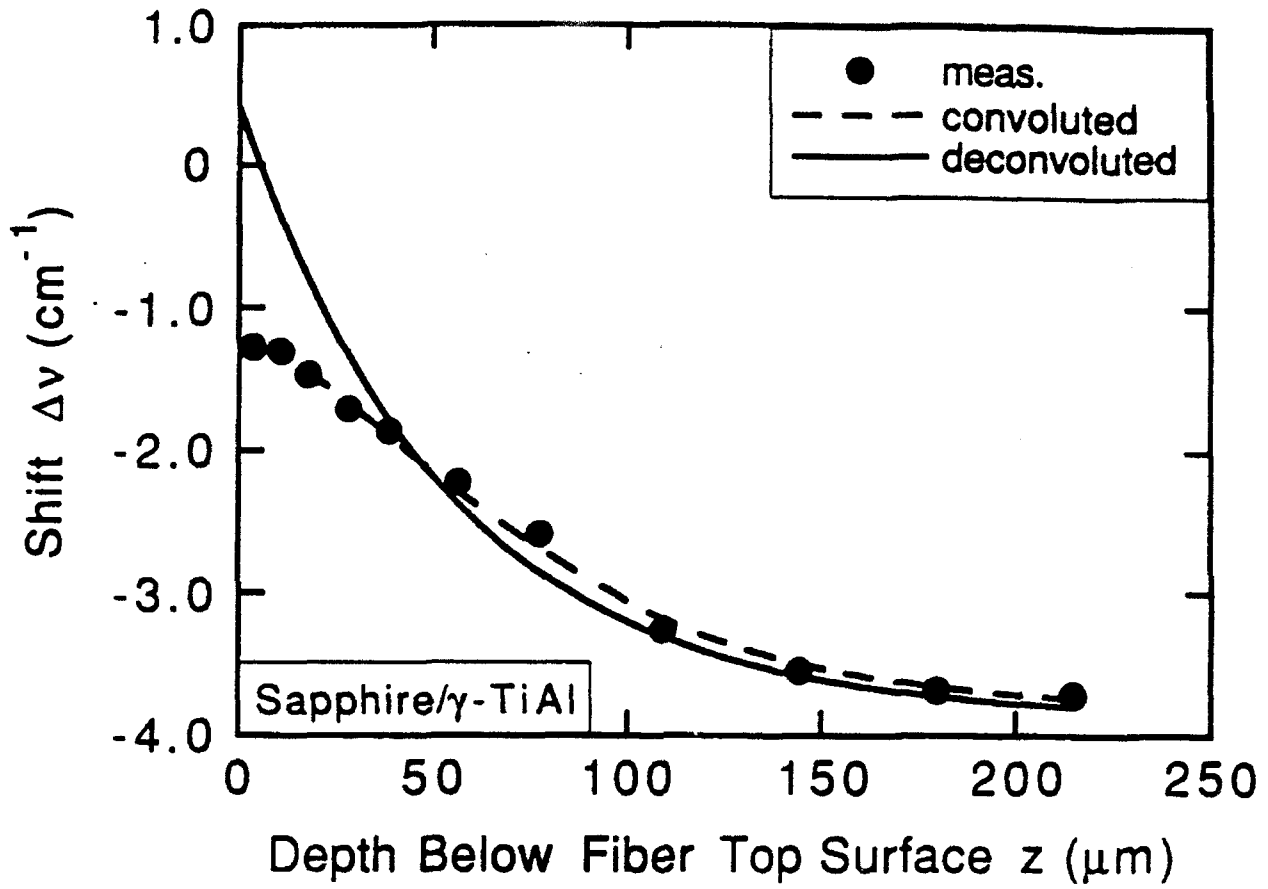


Fig. 5

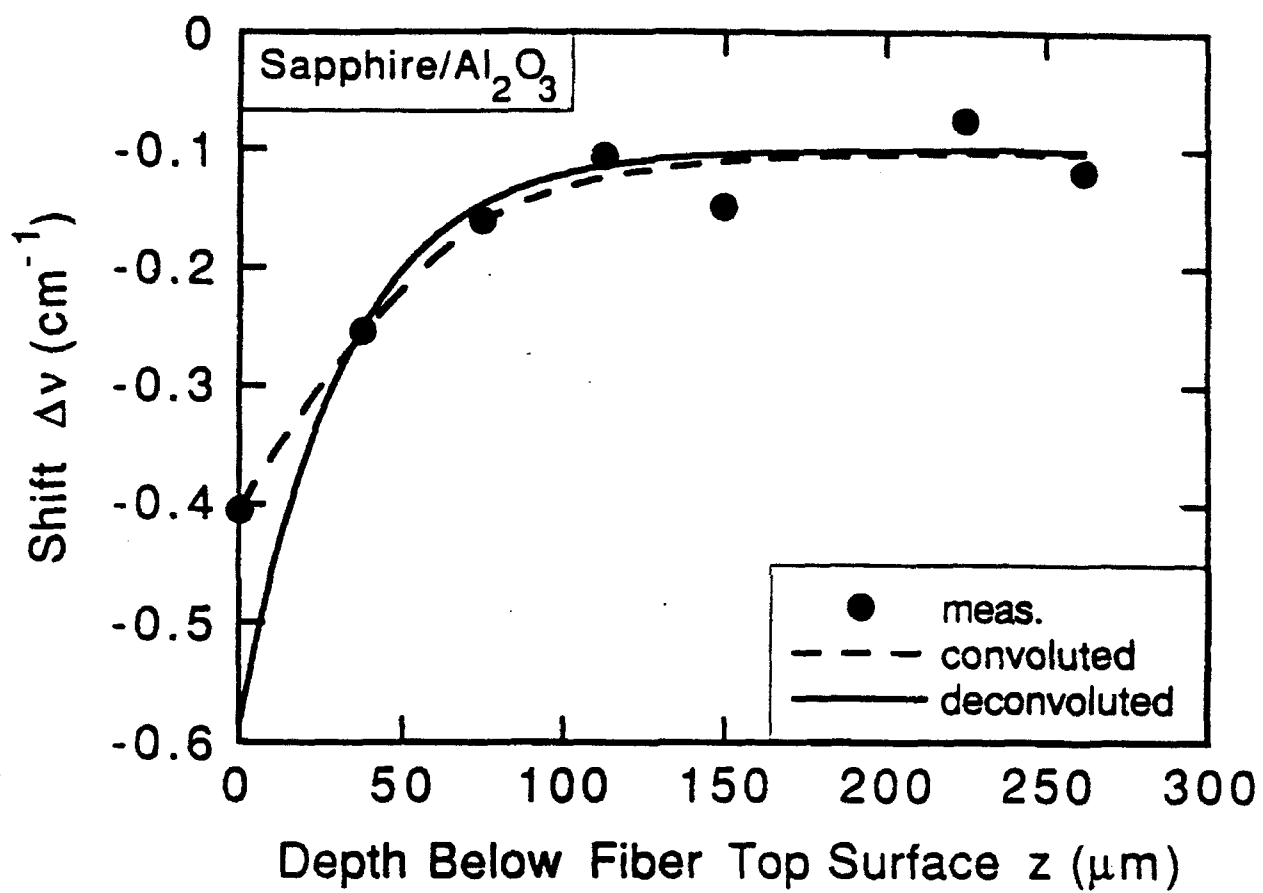


Fig. 6

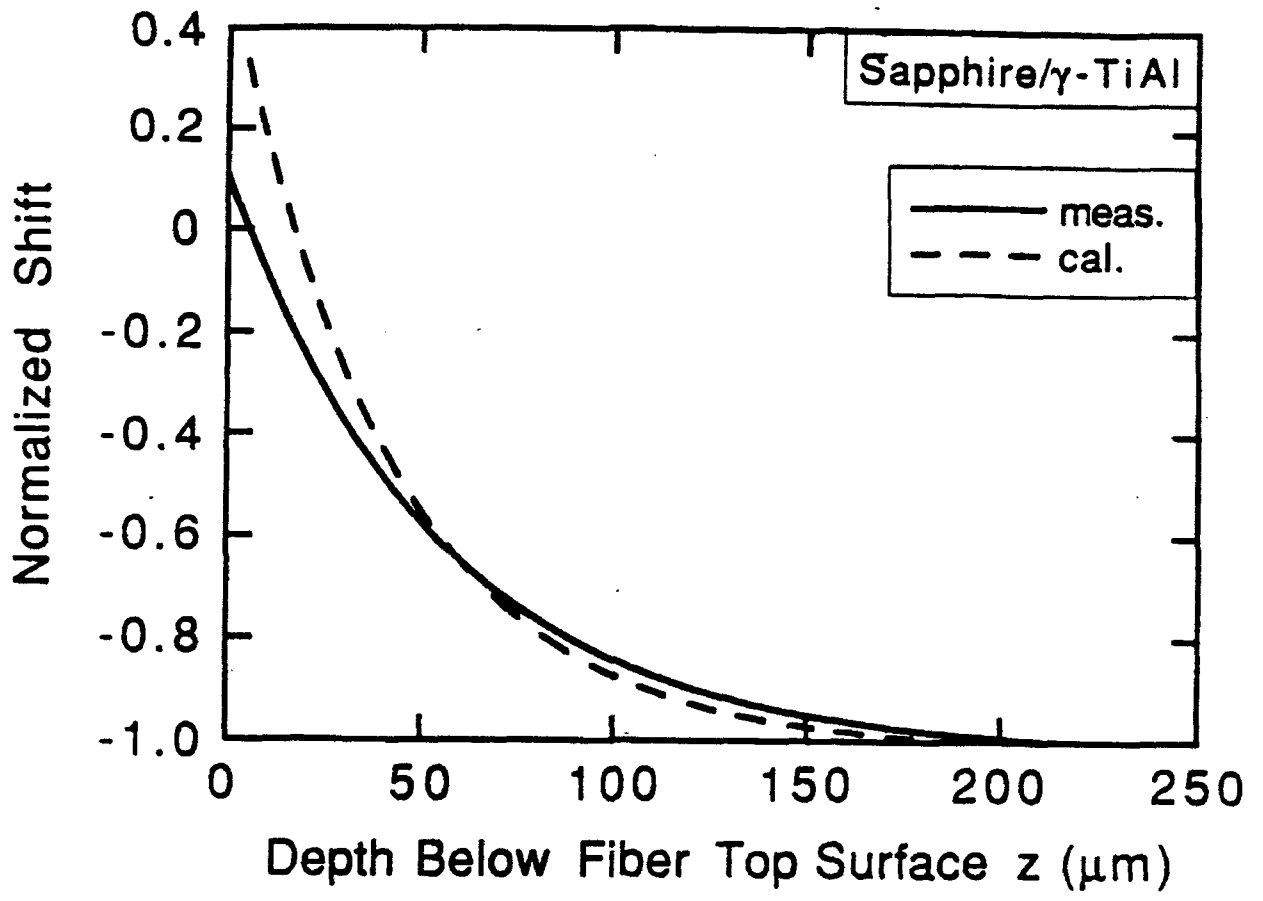


Fig. 7

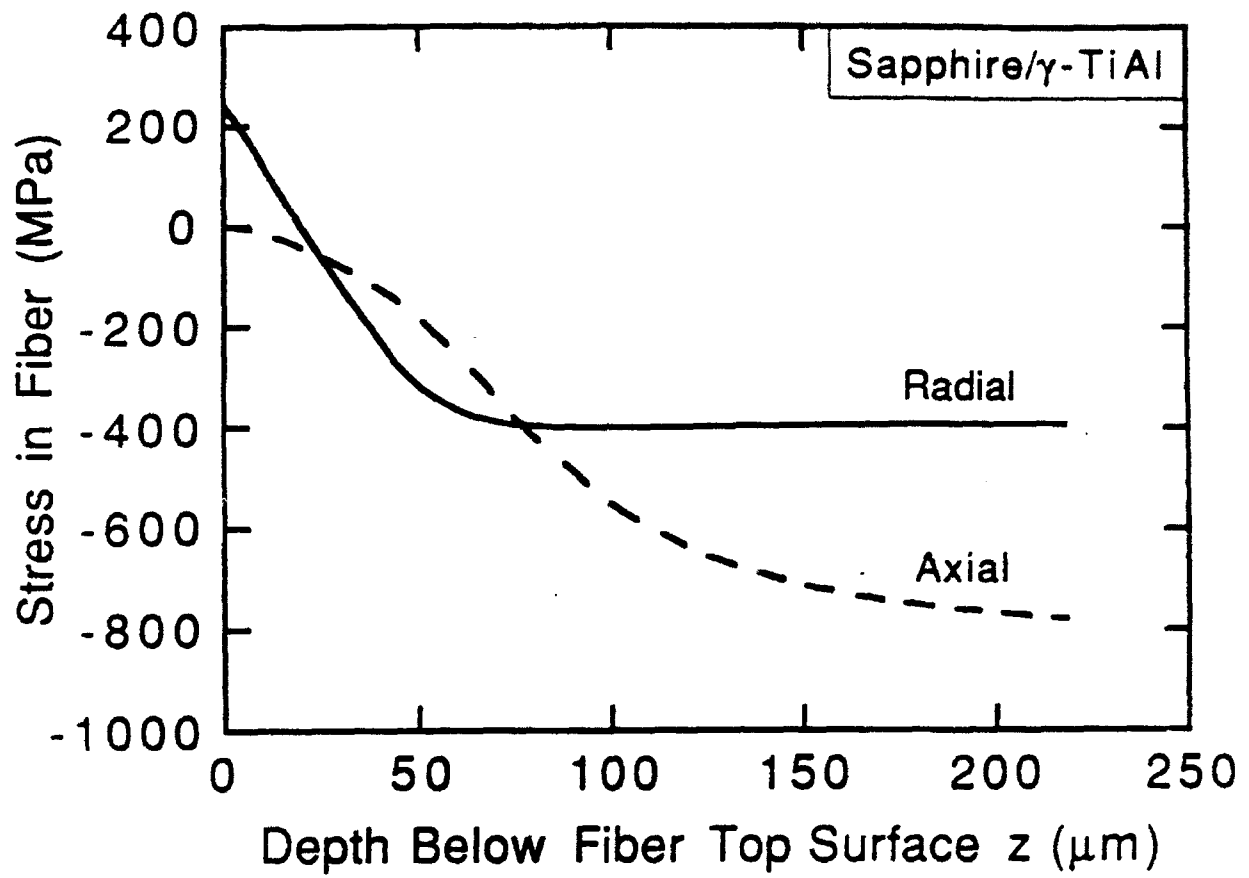


Fig. 8

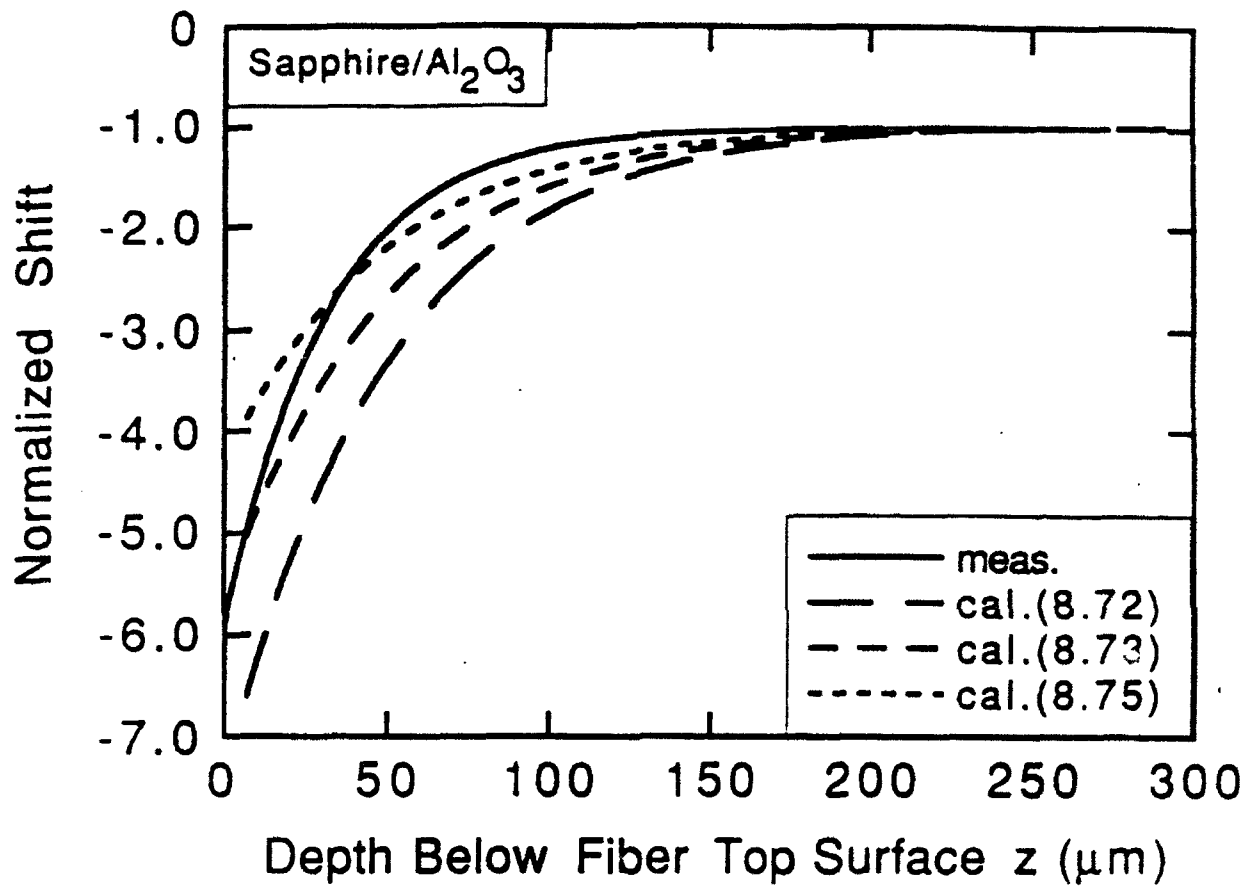


Fig. 9

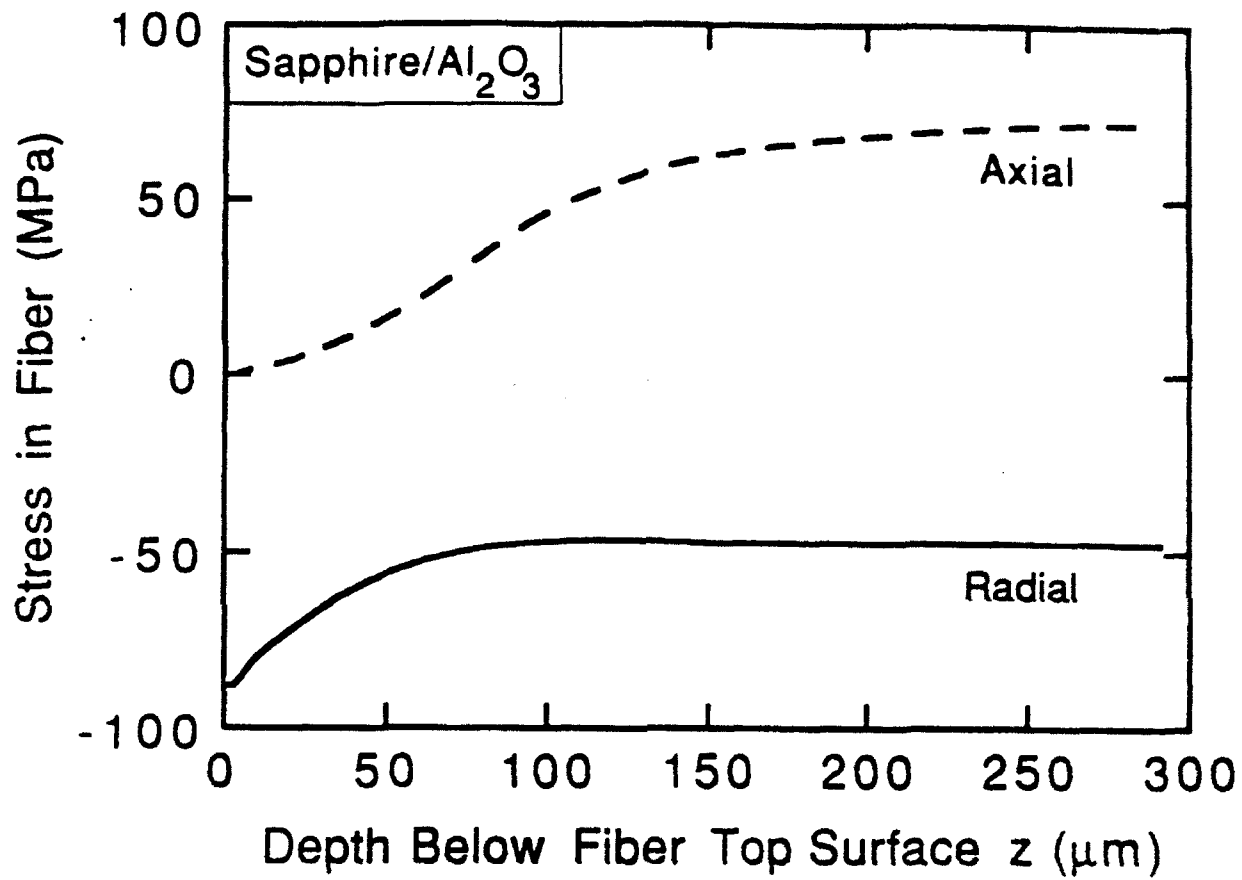


Fig. 10

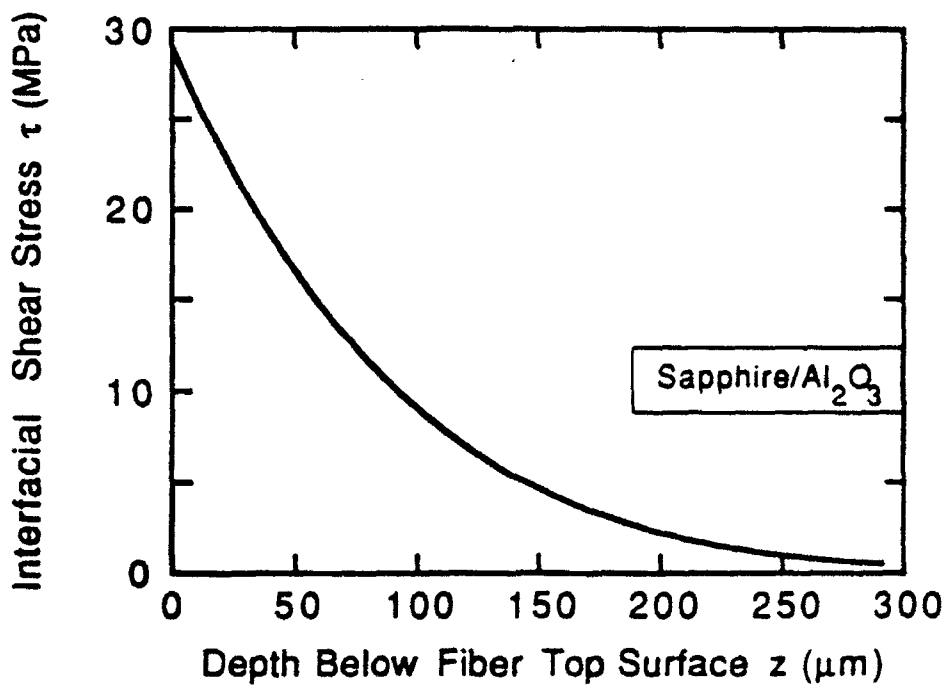
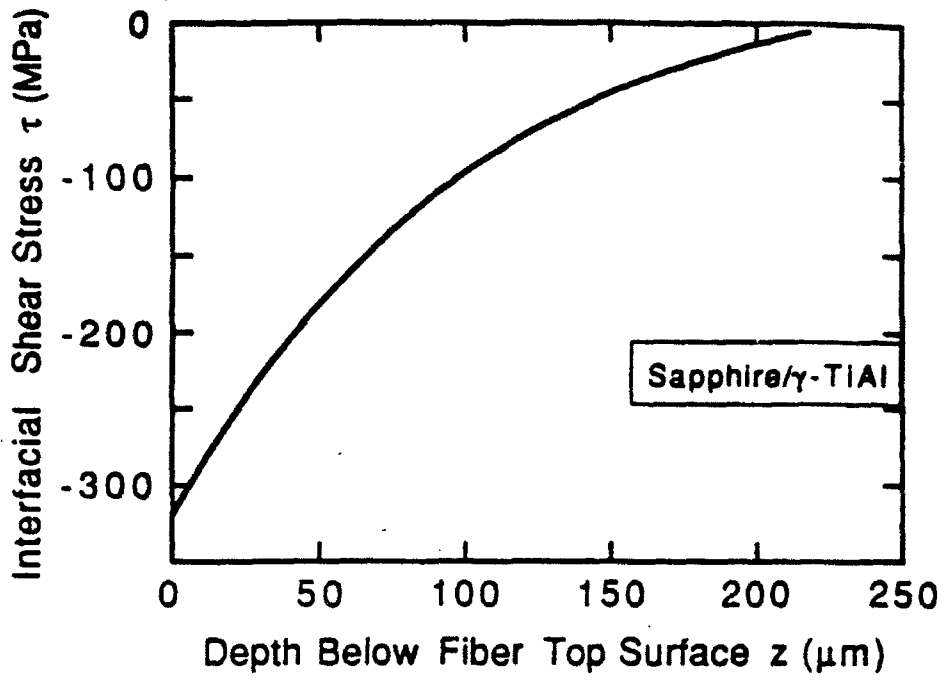
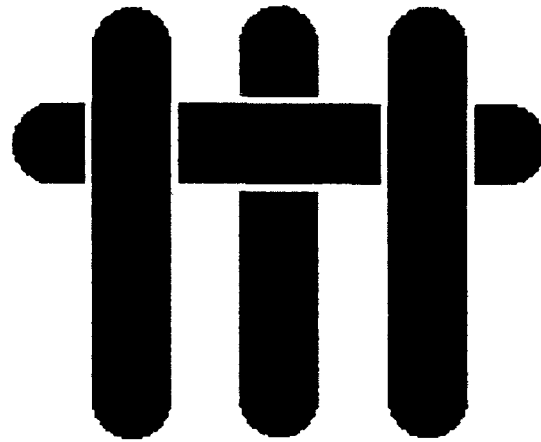


Fig. 11

**MATERIALS UCSB**



**Optical Fluorescence from Chromium Ions in  
Sapphire: A Probe of the Image Stress**

by

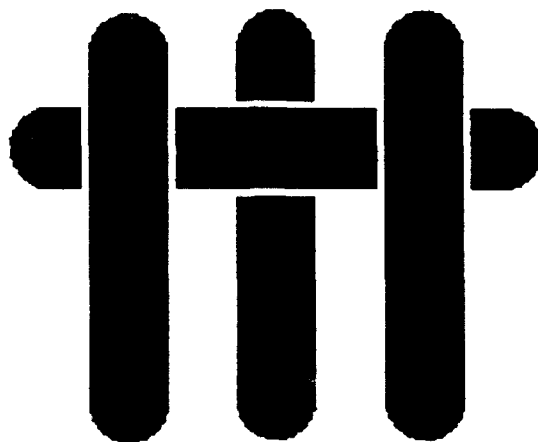
**Qing Ma and David R. Clarke  
Materials Department  
University of California, Santa Barbara**

**A Technical Report for:**

**Office of Naval Research**

**Contract No. N00014-91-J-1875**

**Principal Investigator: David R. Clarke  
Materials Department  
University of California  
Santa Barbara, CA 93106**



**Optical Fluorescence From Chromium Ions In Sapphire:  
A Probe Of The Image Stress.**

Qing Ma and David R. Clarke  
Materials Department,  
University of California,  
Santa Barbara, CA 93106

**Abstract.**

The concentration dependent frequency shift of the fluorescence from chromium ions in sapphire is shown to be a direct probe of the image stress produced by the chromium substituting for the smaller aluminum ions in sapphire. Our analysis is based on a comparison of the frequency shifts produced when the volume of a sapphire crystal is changed by an external pressure to that produced by a concentration of substitutional solute. The volumetric strain sensed by the fluorescing chromium ion when the lattice is expanded by substitutional solute is approximately one-third of that determined from X-ray lattice parameter measurements, in accord with the Eshelby analysis of the strain field due to a concentration of elastic defects in a finite body.

# 1 Introduction

The question as to the lattice distortions produced in a crystal by a substitutional solute is of long-standing interest, and has been the subject of considerable intellectual inquiry. Although it has been recognized throughout that the only proper description is one that takes account of the atomic nature of the solute and the appropriate inter-atomic potentials, early investigators did not have available to them this information. In the absence of such information, it was necessary to address the question using continuum descriptions of the solute and its effect on the lattice. One approach, that might be termed the elastic defect model, was to consider a solute as a center of dilatation supplemented by point singularities of higher order. This enabled the methods of continuum elasticity pertaining to centers of pressure to be employed in finding solutions. For example, Bilby modeled an interstitial atom as a misfitting elastic sphere forced into a smaller hole in a material, and derived solutions for the interaction of a solute with a dislocation [1]. Later, Eshelby, in one of the classic papers in materials, provided a rigorous foundation for the elastic defect model by deriving the forces acting on an elastic singularity in a solid [2]. In subsequent seminal papers [3-5], Eshelby set forth a comprehensive framework for the computation of elastic displacements, strains and stresses resulting from the presence of point defects, inclusions, precipitates and transforming regions. By envisaging a series of hypothetical cutting, transforming and welding operations, and the forces and displacements involved, Eshelby formulated analytical expressions for the stresses and strains created by a region transforming but constrained by a surrounding matrix.

Two concepts introduced by Eshelby are of particular importance. One is that inside any finite body containing defects there exists an additional displacement field, and by extension

strain and stress field, that arises from the boundary condition that at the surface of the body the normal stress must be zero. By analogy with electromagnetic fields, Eshelby termed this additional elastic field the image field. The image field is independent of position inside the body and independent of the size of the body. The second key concept was that of the "stress-free" strain, the shape change of the transforming region that would have occurred in the absence of any constraint. (This same strain has been denoted as the "eigenstrain" by Mura [6], It also appears as the "natural" strain in recent literature on the virtual crystal approximation (VCA) approach to electronic structure calculations [7].) Using the concept of a stress-free transformation strain, Eshelby was able to derive general expressions for the strains produced in the matrix as a result of the transformation as a function of the shape of the ellipsoidal inclusion. The matrix strain is shown to consist of two components, the strain in the matrix if it were of infinite extent and the image strain.

The existence of two components to the strain field in a body containing defects naturally raises the question as to which strains are actually being determined when measuring the lattice parameter by diffraction methods. Although there was, for a period, considerable confusion concerning this question, it now appears resolved that Bragg diffraction methods, using X-rays and neutrons, provide a direct measure of the spatially averaged total strain in the body. (Diffuse scattering provides additional information on the distribution of the lattice distortions but does not include information about average lattice strain.) Since the image strain was shown by Eshelby to be a constant fraction of the total strain, the magnitude of the image strain has been deduced from the concentration dependence of the lattice parameter. However, there have not been, as far as the authors are aware, any direct measurements of the image strain.

In the course of rather different studies [8-10], directed towards the application of optical

fluorescence methods to the measurement of stresses in composite materials, we have, we believe, found that the fluorescence from substitutional solutes of chromium directly probes the image stress in single crystals of sapphire ( $\text{Al}_2\text{O}_3$ ). In this short paper, we describe how we reached this conclusion. It is first necessary, however, to re-examine the data in the literature on the chromium solid solution in aluminum oxide, together with our own experimental data.

## 2 Chromium Substitution in Sapphire

Solid solutions of chromium in aluminum oxide provide a rich data base to re-examine the question of the short-range and long-range distortion induced by the substitution of a mis-fitting solute. In the literature there exist data on the chromium concentration dependence of density [11], lattice parameter determined by X-ray diffraction [11], and frequency of characteristic optical fluorescence lines [12]. In addition, both lattice parameter and fluorescence line shifts as a function of hydrostatic pressure have been reported for selected chromium ion concentrations [13-15]. The system  $\text{Al}_2\text{O}_3\text{-Cr}_2\text{O}_3$  also has the advantage that there is complete solid solution between the two oxide phases [16].

The substitutional nature of the chromium ion has been confirmed by density and X-ray measurements (below). This is consistent with both the existence of the continuous solid solution with  $\text{Cr}_2\text{O}_3$ , the similarity in ionic radius between  $\text{Cr}^{3+}$  (0.064 nm) and  $\text{Al}^{3+}$  (0.057 nm), and the fact that the corundum structure is a rather close-packed structure and does not contain any interstices as large as the chromium ion. Structure analysis as a function of hydrostatic pressure further shows that the corundum structure of sapphire compresses uniformly, with all the distances decreasing equally and all the interatomic angles remaining unchanged [17].

Chromium in sapphire is also a chromophore, giving rise to the characteristic red fluorescence of ruby. The fluorescence originates from electronic transitions in the chromium ion produced by appropriate excitation. Electrons excited from their ground state,  $^4A_2$ , can lose their excess energy by a variety of radiative (and non-radiative) processes. The most pronounced transitions being the R-fluorescence lines at 1.790 and 1.794 eV in the red. (A recent paper tabulates all the radiative transitions in the visible part of the spectrum [18]). The chromium ion can substitute for any of the aluminum ions in the corundum crystal structure of sapphire with the result that they are octahedrally coordinated to neighboring oxygen and aluminum ions. The octahedron is not regular, but elongated along the *c*-axis of the lattice, resulting in splitting of the R-fluorescence lines to form the doublet of  $R_1$  and  $R_2$  lines. X-ray refinements [19,20], in highly doped (4a/o Cr) sapphire show the chromium ion to be slightly displaced along the *c*-axis from the position normally occupied by the aluminum ion so that the chromium site symmetry is further reduced, but nevertheless retains a three fold rotational symmetry about the *c*-axis. The effect of an applied stress is to distort the crystal field surrounding the chromium ion, change its potential energy and thereby alter the energies of the radiative transitions.

## 2.1 Optical Fluorescence Data

The frequencies of the  $R_1$  and  $R_2$ , as well as the extended neighbor fluorescence N lines, have all been reported to shift with pressure and with chromium concentration. The pressure dependence is well known [13,14] and continues to be subject to further refinement because of its central importance as a pressure gauge for high pressure studies. The reported pressure

dependence of the frequency shift  $\Delta\nu$  may be expressed as:

$$\Delta\nu = -(2\Pi_{11} + \Pi_{33})P \quad (1)$$

where  $\Pi_{i,j}$  is the piezo-spectroscopic coefficient. The original work of Forman *et. al.* [13] is reproduced in figure 1a for the  $R_1$  line with the sum  $2\Pi_{11} + \Pi_{33}$  having a value of  $7.7 \text{ cm}^{-1}\text{GPa}^{-1}$ . The results for  $R_2$  line is very similar and therefore not included here. Recent work, examining the fluorescence from beams loaded in four point bending, has shown that the equation is equally valid for tension [8,9].

The chromium concentration dependence of the fluorescence energy has been the subject of just one previous study [12]. Our own results have proven to be essentially identical to those of Kaplyanskii *et. al.* [12], which are reproduced in figure 1b. The data may be expressed by the linear dependence:

$$\Delta\nu = 99 c_m \quad (2)$$

where  $\Delta\nu$  is measured in wavenumber and  $c_m$  is the chromium concentration (in w/o).

## 2.2 X-ray Lattice Parameter Measurements

X-ray lattice parameter measurements have been made as a function of pressure on rubies with a number of different chromium concentrations [15,17,18]. These studies indicate an isotropic compressibility with the interatomic distances decreasing equally with pressure and the interatomic angles remaining unchanged up to at least 4.6 GPa [17]. The results of

d'Amour *et. al.* [15] is shown in figure 1c, which can be fitted to the following linear relations:

$$a = 0.47664(1 - 0.001173 P)$$

and

$$c = 1.3007(1 - 0.001332 P) \quad (3)$$

where the lattice parameters  $a$  and  $c$  are measured in nanometers, and  $P$  is measured in GPa. They also found that the density increased with increasing pressure according to the Murnaghan equation of state.

The X-ray lattice parameter measurements were also made as a function of chromium concentration [11] (figure 1d), over a range of chromium concentration up to 2 w/o by Jan *et. al.* They indicate that the lattice parameters and derived density are given by the linear relationships:

$$a = 0.47591(1 + 0.0527 c_m)$$

$$c = 1.29894(1 + 0.0452 c_m)$$

and

$$\rho_X = 3.9864(1 + 0.340 c_m) \quad (4)$$

where the density  $\rho_X$  is measured in  $\text{g}/\text{cm}^3$ .

### 2.3 Density Data

Jan *et. al.* have also made precision density measurements [11] using the picnometry technique. Their results indicate a linear dependence of the density on the chromium con-

centration given by the relationship:

$$\rho = 3.9860(1 + 0.341c_m) \quad (5)$$

The linear dependence, as clearly shown in figure 2, is consistent with chromium being a substitutional solute [21]. The physical density determined above is, within experimental error, the same as the X-ray density measurements by Jan *et. al.* in equation 4. This demonstrates the equivalence of the solute induced macroscopic strain and the mean strain measured by X-ray.

#### 2.4 Frequency Shift as a Function of Mean Strain

From the results presented in figure 1, the frequency shift can be related to the mean volumetric strain  $\Delta V/V$  by using the following relationship:

$$\frac{\Delta V}{V} = 2 \frac{\Delta a}{a} + \frac{\Delta c}{c}$$

Therefore, from equations 1 and 3, and equations 2 and 4, we obtain the following expressions for the fluorescence shifts:

$$\begin{aligned} \Delta\nu^P &= 2100 \frac{\Delta V}{V} \\ \Delta\nu^D &= 660 \frac{\Delta V}{V} \end{aligned} \quad (6)$$

depending on whether the strain is produced by an external pressure or by solute doping. The superscripts  $P$  and  $D$  denote pressure and solute doping respectively.

### 3 Analysis and Discussion

The intriguing feature of the data assembled in the previous section is that the apparent strain sensed by a fluorescing chromium ion is different depending on whether the lattice is strained by the application of a hydrostatic pressure or internally by the addition of substitutional solute. Specifically, for the same lattice strain measured by changes in the lattice parameter by X-ray diffraction the frequency shift of the chromium line produced by doping is about one-third (equation 6) that produced by an applied pressure:

$$\Delta\nu^D \sim \frac{1}{3} \Delta\nu^P \quad (7)$$

We believe that the different pressure and solute concentration effects may be reconciled by postulating that the frequency shift of the fluorescence lines is sensitive to the image strain whereas X-ray diffraction monitors the average lattice strain. To prove this, we proceed to perform a set of imaginary experiments (figure 3), assuming for simplicity that the medium is elastically isotropic and that the concentration of solute is sufficiently small that any solute interaction effects, such as dipolar or higher, can be ignored.

We start with a body of sapphire of volume  $V$ , free of external pressure ( $P = 0$ ), containing only a few  $\text{Cr}^{3+}$  ions to sense the strain, so that the solute concentration  $f \rightarrow 0$ . The frequency of the fluorescence line is

$$\nu = \nu(P = 0, f \rightarrow 0) \quad (8)$$

This frequency is expected to be, in the complicated manner, dependent on the local strain in the vicinity of each  $\text{Cr}^{3+}$  ion as it is a substitutional solute, larger than the  $\text{Al}^{3+}$  ion it

replaces. Fortunately, by choosing this state as the reference state, a knowledge of the effect of this local strain is unimportant since it is the same for both the state of interest and the reference state and hence cancels out.

In the first experiment, a hydrostatic tensile stress  $-P$  is applied to the body, so that its volume increases by  $\Delta V$ . The strain dependence (due to an applied stress  $-P$ ) of the frequency shift [9] for an isotropic material can be in general expressed as

$$\Delta\nu = \lambda \epsilon_{ii} \quad (9)$$

where the convention of summation of repeated indices is assumed and where  $\lambda$  is the piezo-spectroscopic volumetric strain coefficient. Therefore, the frequency shift due to the stress  $-P$  is simply

$$\begin{aligned} \Delta\nu^P &= \nu(-P, f \rightarrow 0) - \nu(P = 0, f \rightarrow 0) \\ &= \lambda \frac{\Delta V}{V} \end{aligned} \quad (10)$$

Alternatively, in the second experiment, we can produce such a volume change by increasing the number of  $\text{Cr}^{3+}$  ions in the body from virtually zero in our reference state to  $N$ , distributed at random. Following Eshelby, the displacement field generated in an infinite body by all the substitutional ions may be written as:

$$\bar{u}^\infty(\bar{r}) = C \sum_n^N \frac{\bar{r} - \bar{r}_n}{|\bar{r} - \bar{r}_n|^3} \quad (11)$$

where  $C$  is the dilational strength of an individual  $\text{Cr}^{3+}$  ion, proportional to its misfit.

In a finite crystal, the displacements are modified by the existence of the image term,

required so that the tractions at the external surface are zero. The additional displacement at position  $\vec{r}$  produced by the image force is [3]:

$$\vec{u}^{im}(\vec{r}) = \frac{8\pi(1-2\sigma)}{3(1+\sigma)} \frac{CN}{V} \vec{r} \quad (12)$$

where  $\sigma$  is Poisson's ratio. The total displacement is then the sum of these two displacements:

$$\vec{u}^{total}(\vec{r}) = C \sum_n \frac{\vec{r} - \vec{r}_n}{|\vec{r} - \vec{r}_n|^3} + \frac{8\pi(1-2\sigma)}{3(1+\sigma)} \frac{CN}{V} \vec{r} \quad (13)$$

The volume change produced by the solute is then simply the integral of the displacement field over the surface of the body:

$$\begin{aligned} \Delta V &= \int_V \vec{u}^{total}(\vec{r}) \cdot d\vec{s} \\ &= 4\pi C N \frac{3(1-\sigma)}{1+\sigma} = 4\pi C N \gamma \end{aligned} \quad (14)$$

From this volume change, the mean strain in the body produced by solute doping is:

$$\bar{\epsilon}_{ii} = \frac{\Delta V}{V} = 4\pi\gamma C \frac{V}{V} = 4\pi\gamma C f \quad (15)$$

where  $f$  is the concentration of  $\text{Cr}^{3+}$ .

However, the strain field sensed by an individual substitutional ion is different from that described above as we now show. Consider a small but finite volume element,  $W$ , of arbitrary size but which does not contain any solute ions other than a single probe ion whose fluorescence we may use to monitor the state of this small volume element. The volume expansion (due to doping in the body) of this element of volume may be written as before

as:

$$\Delta W = \int_W \vec{u}^{total}(\vec{r}) \cdot d\vec{s} - \int_W \vec{u}^{probe}(\vec{r}) \cdot d\vec{s} \quad (16)$$

In this equation, the first term gives the contribution of the total displacement field, which includes the image term due to all substitutional ions (equation 12), and the displacement field due to the probing ion itself, since the displacements due to other ions in equation 11 not included in  $W$  do not contribute to the integration. Because the displacements generated by the probing ion are already in the reference state, to which the volume change is being compared, its contribution is subtracted by the second term in the equation 16. So, effectively, only the image displacement field due to the presence of all substitutional ions in the body contributes to  $\Delta W$ . We may then write:

$$\Delta W = \frac{8\pi(1-2\sigma)}{1+\sigma} WCf \quad (17)$$

Therefore, the strain sensed by the solute ion is simply the image strain:

$$\epsilon_{ii}^{im} = \frac{\Delta W}{W} = 4\pi(\gamma-1)Cf \quad (18)$$

Comparing with equation 15, the corresponding frequency shift of the fluorescence from the sensing solute ion would then be:

$$\begin{aligned} \Delta\nu^D &= \nu(P=0, f = \frac{N}{V}) - \nu(P=0, f \rightarrow 0) \\ &= \lambda \epsilon_{ii}^{im} = \lambda \frac{\gamma-1}{\gamma} \bar{\epsilon}_{ii} = \lambda \frac{\gamma-1}{\gamma} \frac{\Delta V}{V} \end{aligned} \quad (19)$$

If one assumes that the Poisson's ratio is 1/3, then a comparison of equations 10 and 19 indicates that the effect of solute concentration on the fluorescence shift is about 1/3 that

produced by an external pressure, as found experimentally (equation 6). Since in the case of solute concentration, the strain affecting the shift is entirely due to the image term, we therefore conclude that the fluorescence probes the image strain whereas X-ray diffraction provides a measurement of the total strain.

## ACKNOWLEDGEMENT

This work was supported by the Office of Naval Research under grant N00014-91-J-1875. The authors are grateful to Dr. I. Tanaka, Osaka University, for providing a number of the synthetic rubies used in this work.

## References

1. B. A. Bilby, *Proc Phys. Soc.* A63, 191 (1950).
2. J. D. Eshelby, *Phil. Trans. Royal Society*, A244, 87 (1951).
3. J. D. Eshelby, *Journal of Applied Physics*, 25, 255 (1954).
4. J. D. Eshelby, in *Solid State Physics* (ed. by F. Seitz and D. Turnbull), 3, 79 Academic Press, New York (1956).
5. J. D. Eshelby, *Proceedings of the Royal Society*, A241, 376 (1957).
6. T. Mura, *Micromechanics of Defects in Solids*, Martinus Nijhoff Publishers, Hague (1982).
7. J.L. Martin and A. Zunger, *Phys. Rev. B* 30, 6217 (1984).
8. S. E. Molis and D. R. Clarke, *Journal of the American Ceramic Society*, 73, 3189 (1990).
9. Q. Ma and D. R. Clarke, *Journal of the American Ceramic Society*, submitted.
10. Q. Ma and D. R. Clarke, to be published.
11. J.-P. Jan, S. Steinemann and P. Dinichert, *Helv. Phys. Acta*, 33, 123 (1960).
12. A. A. Kaplyanskii, A. K. Przhevuskii and R. B. Rozenbaum, *Soviet Physics-Solid State*, 10, 1864 (1969).
13. R.A. Forman, G.J. Piermarini, J.D. Barnett and S. Block, *Science*, 176, 284 (1972).
14. G. J. Piermarini, S. Block, J. D. Barnett and R. A. Foreman, *Journal of Applied Physics*, 46, 2774 (1975).
15. H. D'Amour, D. Schiferl, W. Denner, H. Schulz and W. B. Holzapfel, *Journal of Applied Physics*, 49, 4411 (1978).
16. *Phase Diagrams for Ceramists*, The American Ceramic Society, Columbus, Ohio (1969).
17. L.W. Finger and R. M. Hazen, *Journal of Applied Physics*, 49, 5823 (1978).
18. J.H. Eggert, K.A. Goettel, and I.F. Silvera, *Physical Review B* 40, 5724 (1989).

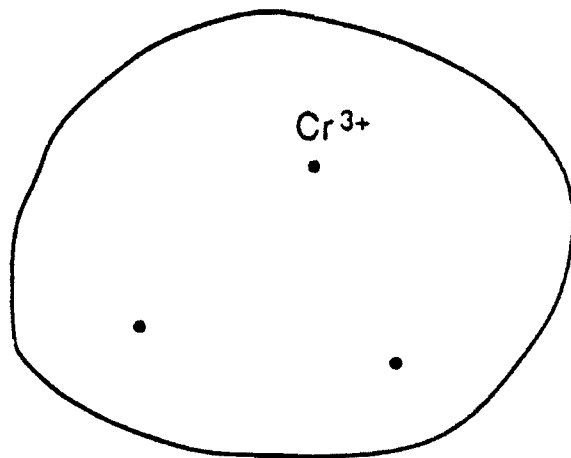
19. S. C. Moss and R. E. Newnham, *Zeitschrift fur Kristallography*, 120, 359 (1964).
20. J. W. McCauley and G. V. Gibbs, *Zeitschrift fur Kristallography*, 135, 453 (1972).
21. R. W. Balluffi and R. O. Simmons, *Journal of Applied Physics*, 31, 2284 (1960).

## Figure Captions

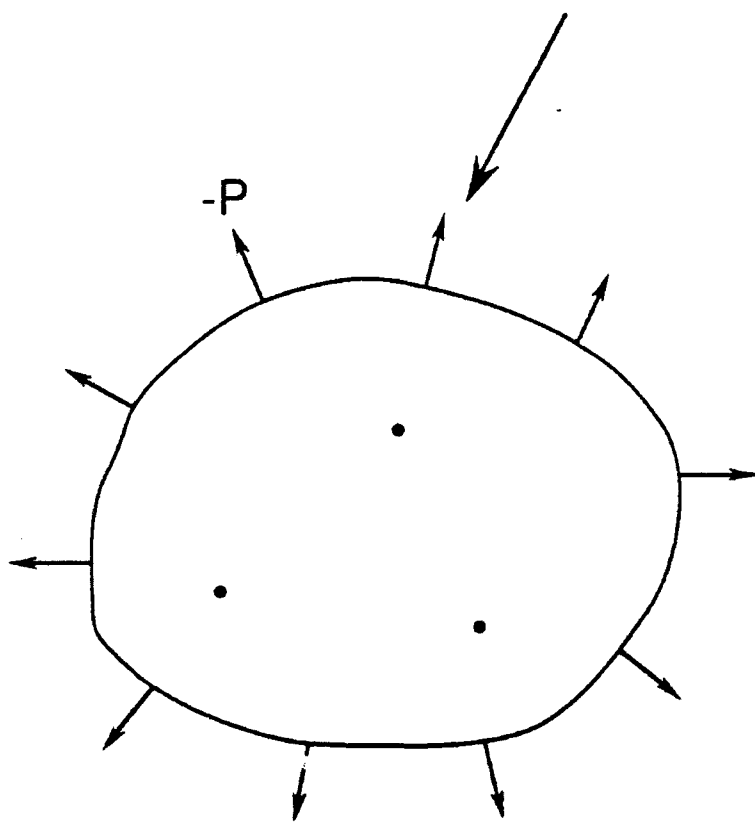
Figure 1. Data on the chromium solid solution in aluminum oxide. (a) Pressure dependence of frequency shift for the  $R_1$  fluorescence line [13]. (b) Concentration dependence of frequency shift for the  $R_1$  fluorescence [12] line. (c) Pressure dependence of the lattice parameters of sapphire [15]. (d) Concentration dependence of the lattice parameters of sapphire [11].

Figure 2. Linear dependence of the density of alumina oxide on the chromium concentration [11].

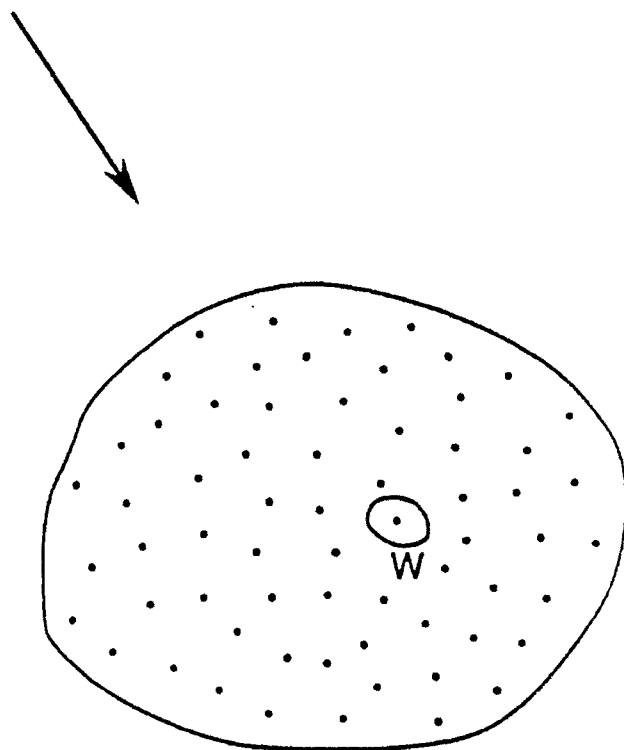
Figure 3. Illustration of a set of imaginary experiments to produce a volume change by either external stress or solute doping. The region  $W$  is small but finite volume of arbitrary size that contains a single probe ion used to monitor the strain.



REFERENCE STATE:  $V, P = 0, f \rightarrow 0$



$V + \Delta V, -P, f \rightarrow 0$



$V + \Delta V, P = 0, f = N/V$

